Climate Dynamics (1988) 3:45–84

Climate Dynamics

The dynamical range of global circulations — II

Gareth P Williams

Geophysical Fluid Dynamics Laboratory/NOAA, Princeton University, Princeton, NJ 08542, USA

Abstract. The dynamical range of global atmospheric circulations is extended to specialized parameter regions by evaluating the influence of the rotation rate (Ω) on axisymmetric, oblique, and diurnally heated moist models. In Part I, we derived the basic range of circulations by altering Ω for moist and dry atmospheres with regular and modified surfaces. Again we find the circulations to be composed of only a few elementary forms. In axisymmetric atmospheres, the circulations consist of a single jet in the rotational midrange ($\Omega^* = \frac{1}{2}$–1) and of double jets in the high range ($\Omega^* = 2$–4), together with one or two pairs of Hadley and Ferrel cells; where $\Omega^* = \Omega/\Omega_E$ is the rotation rate normalized by the terrestrial value. These circulations differ from those predicted by first-order symmetric-Hadley (SH_1) theory because the moist inviscid atmosphere allows a greater nonlinearity and prefers a higher-order meridional mode. The axisymmetric circulations do, however, resemble the mean flows of the natural system — but only in low latitudes, where they underlie the quasi-Hadley (QH) element of the MOIST flows. In midlatitudes, the axisymmetric jets are stronger than the natural jets but can be reduced to them by barotropic and baroclinic instabilities. Oblique atmospheres with moderate to high tilts ($\theta_p = 25°$–$90°$) have the equator-straddling Hadley cell and the four basic zonal winds predicted by the geometric theory for the solstitial-symmetric-Hadley (SSH) state: an easterly jet and a westerly tradewind in the summer hemisphere, and a westerly jet and an easterly tradewind in the winter hemisphere. The nonlinear baroclinic instability of the winter westerly produces a Ferrel cell and the same eddy fluxes as the quasi-geostrophic QG_2 element, while the instability of the summer easterly jet produces a QG-Hadley (QGH) element with a unique, vertically bimodal eddy momentum flux. At high θ_p and low Ω^*, the oblique atmospheres reach a limiting state having global easterlies, a pole-to-pole Hadley cell, and a warm winter pole. At low tilts ($\theta_p < 10°$), the oblique circulations have a mix of solstitial and equinoctial features. Diurnal heating variations exert a fundamental influence on the natural-Hadley (NH) circulations of slowly rotating systems, especially in the singular range where the zonal winds approach extinction. The diurnality just modifies the NH element in the upper singular range ($\frac{1}{45} \leqslant \Omega^* \leqslant \frac{1}{16}$), but completely transforms it into a subsolar-antisolar Halley circulation in the lower singular range ($0 \leqslant \Omega^* < \frac{1}{45}$). In the modified NH flows, the diurnality acts through the convection to enhance the generation of the momentum-transferring planetary waves and, thereby, changes the narrow polar jets of the non-diurnal states into broad, super-rotating currents. Circulation theory for these specialized flows remains rudimentary. It does not explain fully how the double jets and the multiple cells arise in the axisymmetric atmospheres, how the QGH element forms in the oblique atmospheres, or how waves propagate in the slowly rotating diurnal atmospheres. But eventually all theories could, in principle, be compared against planetary observation: with Mars testing the QGH elements; Jupiter, the high-range elements; Titan, the equinoctial and solstitial axisymmetric states; and Venus, the diurnally modified NH flows.

1 Introduction

We continue the presentation, begun in Part I (Williams 1988), of the circulation set generated by varying some of the fundamental external pa-

rameters and internal physical factors that control the dynamics of a terrestrial global circulation model (GCM). The solutions are developed for two purposes: (1) to study basic circulation dynamics by altering the scale and mix of the jets, cells and eddies; and (2) to broaden the perspective on planetary and terrestrial climates by defining the dynamical range and the parametric variability of global circulations. In presenting the solutions, we again explore the hypothesis that circulation variability is limited to the mix of a few elementary components that can be understood in terms of standard theories.

In Part I, we derived the basic range of circulations by altering the rotation rate (Ω) and, hence, the Rossby and Froude numbers of moist, dry and modified-surface GCMs driven by a symmetric annual-mean heating. The resulting flows were described in terms of four elementary components, and interpreted in terms of standard symmetric-Hadley (SH) and quasi-geostrophic (QG) theories. We found that a natural-Hadley (NH) element and a tropical quasi-Hadley (QH) element prevail at low and high Ω, respectively, and that a momentum-traversing (QG_γ) element and a momentum-converging (QG_β) element occur in baroclinically unstable midlatitudes at medium and high Ω, respectively. The scales and interactions of these elements lack a full theoretical explanation and deviations occur at transitions and at parameter extremes.

Now, in Part II, we extend the parameter range into three specialized regions, all unrelated but all involving some form of latitudinal or longitudinal asymmetry, by evaluating the influence of Ω on axisymmetric, oblique, and diurnally heated GCMs. The three solution sets are obtained for three basic (but diverse) purposes: (1) to isolate the SH modes of the moist GCM; (2) to define the dynamics of the tropical easterly jets; and (3) to examine the transitions undergone by the NH element as $\Omega \to 0$. The solutions also examine how the axisymmetric flows differ from the natural ones when the barotropic and baroclinic instabilities are suppressed, how the solstitial flows differ from the equinoctial ones when an extreme seasonality is allowed, and how the diurnal flows differ from the nondiurnal ones at very low Ω. As in Part I — to which the reader is referred for notation and terminology — we assume that the GCM is valid in these parameter ranges and that a qualitative comparison between the solutions and the theory is meaningful. We also use the same standard methods for defining and analyzing the circulations, although these are clearly less useful for the eddy-free axisymmetric states and the eddy-dominant Halley flows.

We begin in § 2 with the AXISYMMETRIC set, created by omitting the large-scale longitudinal variations from the basic GCM and by varying the rotation rate over the main range of interest, from $\Omega^* = \frac{1}{2}$ to 4; where $\Omega^* = \Omega/\Omega_E$ is the rotation rate normalized by the terrestrial value. To explain the solutions, we turn to the first-order symmetric-Hadley (SH_1) theory of Held and Hou (1980) — the most successful attempt at defining the symmetric-Hadley state for Earth's atmosphere since Lorenz's (1969) review (see § I-3.1). This SH_1 theory allows for latent heating implicitly, by localizing the cell upflow at the equator, but moisture is not included in the associated numerical modeling. Our AXISYMMETRIC model, on the other hand, includes latent heating explicitly, so we can define the SH modes of moist atmospheres and estimate their contribution to the natural MOIST circulations.

The AXISYMMETRIC solutions turn out to have a more complex bearing on the MOIST states than expected because the thermodynamic forcing changes greatly — the baroclinicity doubles — when the eddies are suppressed in a model that determines its own surface temperature (T_s). The AXISYMMETRIC solutions are also more complex than the SH_1 states because the meridional circulations are more nonlinear when the free atmosphere is fully inviscid, and when the latent heating amplifies the upflows; the SH_1 theory explains only the simplest symmetric states. Axisymmetric circulations are generally more sensitive than natural circulations to the subgrid formulations and the surface conditions, so bridging the gap between the two systems requires a hierarchy of models with different parameterizations.

We proceed to the OBLIQUE set in § 3 to examine the dynamics of the solstitial circulations. Only the summer flows are really sensitive to the interhemispheric heating asymmetries and, in the solstitial limit, they contain a negative baroclinicity, an unstable easterly jet, and an equator-straddling Hadley cell. To define the main range of solstitial circulations and to isolate their invariants, we vary the obliquity θ_p from 10° to 90° and the rotation rate Ω^* from ½ to 4 for a moist GCM. The equinoctial or minimal-tilt states, on the other hand, are adequately described by a GCM forced by an annual-mean heating, as in Part I.

To understand the OBLIQUE solutions, we must first define the solstitial-symmetric-Hadley (SSH) state for the hot-pole limit by modifying the geometric (equinoctial) SH_1 theory. Then, to

describe the eddy fluxes produced by the nonlinear baroclinic instability of the easterly jet in the summer tropics, we must define a new circulation component — the QG-Hadley (QGH) element — whose eddy fluxes and mean flow are governed, respectively, by quasi-geostrophic and Hadley dynamics. The flow in the winter hemisphere, on the other hand, is described by the standard QG_γ element. Thus, the OBLIQUE circulations contain some new modes and some old, yielding another element whose characteristics must be theoretically understood.

Next, with the DIURNAL set in § 4, we examine how longitudinal heating asymmetries affect the dynamics of the low-Ω^* circulations. Diurnal variations play a fundamental role only in the singular rotation range, $0 \leqslant \Omega^* \leqslant 1/16$, where the motion of the sun across the planet's face is low enough to produce a strongly localized heating. In this range, the nondiurnal NH elements also undergo an asymptotic transition — in which the jet weakens and stops moving poleward — when the Hadley cell reaches the pole. Such NH elements are only modified by the diurnality at the top of the singular range, but are completely transformed into subsolar-antisolar (Halley) flows when the rotation rate drops below $\Omega^* = 1/45$. The diurnal forcing can act either through radiation or convection and so can influence an atmosphere directly at upper or lower levels. To see how the form and location of the forcing affects the flow, we consider a special HIGH-CLOUD model in which an opaque cloud adds an upper-level radiative diurnality to the more prevalent low-level convective component. The DIURNAL states contribute to circulation theory in the low range by displaying a different mix of Hadley modes and planetary waves.

Finally in § 5, we assess the connection between the circulations of the various GCMs and the various planets. The planets can test circulation theory in parameter regions not reached by Earth, while the GCM states can provide preliminary models for systems not yet well observed.

2 AXISYMMETRIC(Ω^*) circulations

To isolate the axisymmetric modes of a moist atmosphere, we evaluate a special version of the basic GCM, activating only the smallest and largest longitudinal wavenumbers of the R42 model: $k_\lambda = 0$ and 42 (see Table I-1 for details). Solutions for this small-sector model, dubbed AXISYMMETRIC(Ω^*) even though small longitudinal variations are allowed, are obtained over $\Omega^* =$ ½–4 for comparison with the main MOIST circulations. We retain the largest k_λ to monitor the flow for shear instabilities and to encourage the development of pointwise convection at ten longitudinal grid points — six more than necessary for the spectral transforms. Convection and gravity waves pervade the AXISYMMETRIC flows and force the model to use a smaller time step and a larger time filter. In one case, when $\Omega^* = 4$, the solar constant must be reduced by 10% to prevent the surface temperatures from exceeding 320 K (see § 3 for the reason).

The AXISYMMETRIC(Ω^*) atmospheres evolve from isothermal initial states into statistically equilibrated, troposphere-stratosphere systems in much the same way at all Ω^*, but they take substantially longer to mature than do the MOIST(Ω^*) atmospheres: about 250 days compared to 100 days (Table 1). Clearly, the Hadley processes need more time to develop an axisymmetric jet than the QG eddies need to create a natural jet, so the MOIST eddies are unlikely to sense the AXISYMMETRIC state in midlatitudes. The AXISYMMETRIC(4) circulation, like the MOIST(8) flow, lacks a simple equilibrium and its global kinetic energy fluctuates by a factor of 3. This circulation, however, has a high-energy anomaly, whereas the MOIST(8) flow has a low one. Thus we define a *typical* average using 100 days of data, and a *variant* average for the 40-day period that differs most from the prevailing norm.

Axisymmetric atmospheres can rarely exist physically, so their models are essentially process, not prediction, models. Consequently, tuning the AXISYMMETRIC radiation, PBL and diffusion parameters to the MOIST(1) values is physically arbitrary, but useful for comparative purposes. Furthermore, the axisymmetric flows also lack a natural horizontal mixing by the planetary waves and, therefore, have a greater dependence on the vertical mixing (Held and Hou 1980, hereafter HH80). Nevertheless, the influence of the horizontal mixing can be examined with "small-eddy" models that reduce the sector gradually towards the axisymmetric limit. But the evaluation of a hierarchy of axisymmetric (or quasi-symmetric) models with a variable sector size, PBL formulation, surface state, or moisture content lies beyond the scope of this study.

We begin the presentation of the AXISYMMETRIC(Ω^*) solutions by outlining how the time- and zonally averaged states progress with Ω^*, and then follow with a more detailed description and theoretical interpretation.

Table 1. AXISYMMETRIC circulations: energy, heat and momentum integrals

Case			Energy					Heat				Momentum				
Ω^*	Δ	τ_f	K_Z	K_E	$P_Z K_Z$	$P_E K_E$	K_Z/K_E	T^b	ρ^b — RAD	$v'T'^{-3}$	$-\omega'T'$	Max[a] torque	$v'M'$	$-\omega'M'$	Max[c] $\lvert u\rvert$	Max $\lvert v\rvert$
4V[a]	F		113	1	534	558	15	248.0[a]	5.8 −788	2	753	75	−39	−25	71	3.8
4	F	720	90	1	7	84	21	248.4[a]	5.6 −776	2	87	−57	−14	−1	44	2.3
2	F	450	212	1	50	88	12	253.6	5.7 −888	3	141	−33	−12	3	72	3.7
1	F	495	491	0.2	−263	29	3	253.7	4.4 −904	0.3	40	−14	−2	−15	92	4.2
½	F	405	740	0.3	132	11	2	253.8	3.8 −917	−0.1	18	12	−1	−31	110	3.8
Units		Days	J kg^{-1}		10^{-6} W kg^{-1}			K	cm 10^{-6} K s^{-1}	10^1 J m kg^{-1} s^{-1}	10^{-2} W m^{-2}	m^2 s^{-2}	10^5 kg^2 m	10^5 s^{-2}	m s^{-1}	

[a] Solar constant reduced by 10‰; [b] Instantaneous value here only; [c] Max denotes local extreme. Global means given in other columns; [d] Eddy integrals denoted symbolically; [e] Variant is high kinetic energy phase of solution at $\Omega^* = 4$

τ_f denotes integration period; Δ denotes integration domain and resolution, see Table 1 of Part I; RAD denotes radiative heating rate

2.1 The AXISYMMETRIC(Ω^*) progression (Figs. 1–4)

The AXISYMMETRIC circulations generally consist of one or two jets and one or two pairs of cells. The mean zonal flows in Fig. 1 go from a single broad westerly jet (plus deep equatorial easterlies) in the Ω^* midrange to paired jets (plus shallow easterlies) in the high range. The meridional flows in Fig. 2 have a complex structure and variability, but essentially consist of primary and secondary pairs of Hadley and Ferrel cells. The AXISYMMETRIC(1) system has an even more complex meridional flow because it lies so close to the double-jet transition.

All AXISYMMETRIC temperature fields in Fig. 3 have three parts: a barotropic tropics, a baroclinic midlatitudes, and a radiative-equilibrium in high latitudes. When Ω^* increases, the barotropic zone shrinks and the baroclinicity strengthens because the cells become narrower and transfer less heat poleward: the gradient over the central zone ($\theta = 30°$–$60°$) goes from 40 K at $\Omega^* = \frac{1}{2}$, to 70 K at $\Omega^* = 4$, in 10-K intervals. The main cell pair lies in the barotropic region and is correlated, in the midrange, with the equatorward half of the jet and, in the high range, with the tropical jet. The shear layer between the high-range jets is barotropically unstable and produces a weak eddy kinetic energy, as does the moist convection at the equator (see Fig. 4d).

The AXISYMMETRIC zonal flows resemble the HH80 numerical solutions in their form and in the way they progress with the Ekman number ($=\kappa_V/fH^2$). Changes produced by decreasing κ_V in the HH80 study parallel changes produced by increasing Ω^* here. But the emergence of the shear layer separating the two high-range jets is not explained by the SH_1 theory because internal, rather than integral, processes are responsible. The AXISYMMETRIC meridional flows also differ from their HH80 theoretical and numerical counterparts, presumably because the GCM is completely moist and completely inviscid above the PBL, and hence more nonlinear. The cells in Fig. 2, and the heat and momentum balances in Figs. 5 and 7, all show that a higher-order mode exists for the meridional circulation: the main cell pair has half the width predicted by the SH_1 theory, suggesting that the second harmonic prevails in these more nonlinear states.

The latent heating contributes to the nonlinearity by intensifying the cells. The SH_1 theory does not allow for such circulation-dependent heating and, therefore, cannot explain the AXI-

SYMMETRIC cells and their complex correlation with the zonal flow and temperature. Paradoxically, the SH_1 mode is better realized in the MOIST NH and QH elements than in the AXISYMMETRIC states — because the horizontal wave mixing reduces the meridional nonlinearity of the natural flows. Although the AXISYMMETRIC states are more complex and more nonlinear, some SH_1 features are discernible: a momentum wind and a Hadley cell in the lowest latitudes, and a radiative thermal wind in the highest latitudes. But the scale of the cells, the strength of the Ferrel cell, and the dynamics of the jet-separation zone remain unexplained.

To compound the problem, the AXISYMMETRIC circulations are also too idiosyncratic to be a good guide to the dynamics of the MOIST mean flows: their jets and baroclinicity are just too strong when the heat transport is so reduced, and their cells are too dependent on factors that vanish when longitudinal variations are allowed. Consequently, the behavior of the baroclinically unstable eddies in a MOIST midrange flow is better revealed by a comparison with a stable low-range flow than with an AXISYMMETRIC flow: the changes produced by varying the rotation rate are less than those produced by suppressing the longitudinal dependence. In the high range, however, the MOIST mean flows can only be usefully compared with their AXISYMMETRIC counterparts. Such a comparison reveals similarities in the low latitudes but large differences in the midlatitudes. In general, comparing the natural and axisymmetric flows is meaningful only when the drag is strong enough to limit the barotropic cascade — see § I-6.

The AXISYMMETRIC process model remains useful, despite the complexity of its circulations, because it describes an intrinsic GCM mode and because it defines the limits of the SH_1 theory. The AXISYMMETRIC solutions represent the complex end of a hierarchy of SH states and suggest that the elements defined in Part I are first-order items at best.

2.2 *The AXISYMMETRIC(Ω^*) basic fields*

Zonal flow. Looking at the midrange solutions in detail, we see from Fig. 1c, d that the jets, like the temperature fields, consist of three parts: a momentum wind u_M in the barotropic tropics, a baroclinic wind in the midlatitudes, and a radiative thermal wind u_E in the high latitudes. The zonal flow matches u_M over the Hadley cell, but drops to $u_M/2$ at the jet peak because of the detrainment and friction in the Ferrel cell. (Note that $a\Omega_E = 465$ ms^{-1}.) The midrange zonal flows, with their broad westerly jets and deep equatorial easterlies, closely resemble the HH80 solutions for a moderate dissipation (or Ekman number). These jets are almost twice as strong as their MOIST counterparts, and would obviously be reduced by the natural shear instabilities.

In the high range, the zonal flow splits into a tropical jet and a midlatitude jet (Fig. 1a, b). These jets separate most completely at $\Omega^* = 2$, connecting only in the stratosphere. The AXISYMMETRIC(4) jets, however, separate less and resemble the HH80 solutions for a low dissipation. The sharp transitions that occur for the AXISYMMETRIC and MOIST systems between $\Omega^* = 1$ and 2 are related, and confirm the importance of the Hadley modes in the natural circulations. But in midlatitudes the two systems differ completely: the AXISYMMETRIC flows are barotropically unstable in the separation zone — see K_E in Fig. 4d and $\{K_Z : K_E\}$ in Table 1 — and baroclinically unstable in midlatitudes, whereas the MOIST flows are only baroclinically unstable. Clearly, the AXISYMMETRIC flows do not provide the basic state for the baroclinic instability. In low latitudes, however, the high-range AXISYMMETRIC and MOIST states have a closer connection, in that the AXISYMMETRIC tropical jet and easterly tradewinds closely resemble the mean zonal flow of the QH element in scale and strength, especially when the MOIST eddies are small, as at $\Omega^* = 4$. But only the equatorward half of the tropical jet relates to u_M; the other half depends on the higher-order effects associated with the Ferrel cell and the separation zone (Fig. 1a).

Meridional flow. According to the SH_1 theory, the meridional circulations should consist of a Hadley cell that extends from the equator to the jet core to form the momentum wind aloft, and of a weak Ferrel cell that lies beneath the jet core. Although the AXISYMMETRIC meridional flows are more complex than this, they do agree with the SH_1 theory in the lowest and highest latitudes — but not in between — and are strongly correlated with the zonal flows and temperatures. The implications of the AXISYMMETRIC solutions for the SH_1 theory are simpler than their bearing on MOIST circulations: they tell us that the theory provides only a first-order description and is limited to minimally nonlinear states.

The AXISYMMETRIC Hadley cell deviates

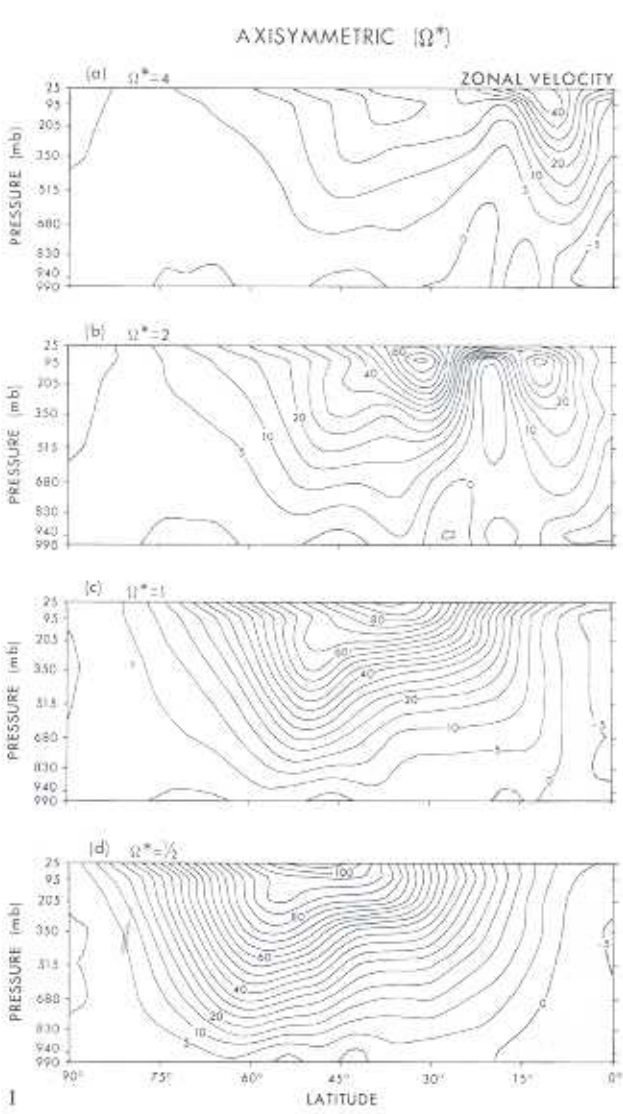

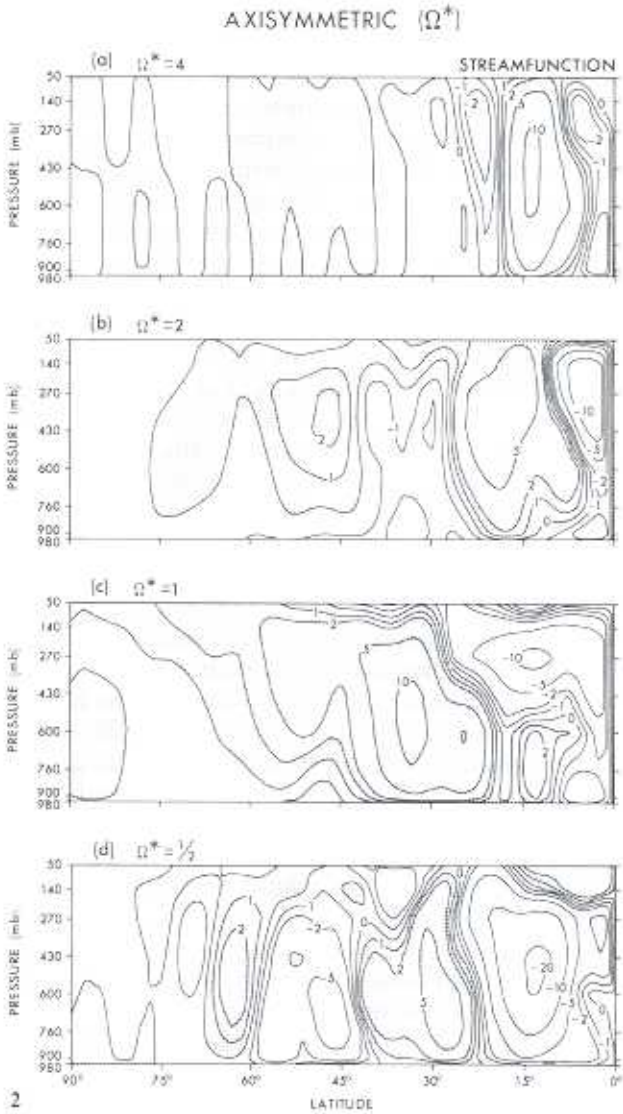

Fig. 1. Meridional distribution of the mean zonal wind for the AXISYMMETRIC model with $\Omega^* = \frac{1}{2}$–4. Units: ms^{-1}

Fig. 2. Meridional distribution of the mean stream function for the AXISYMMETRIC model with $\Omega^* = \frac{1}{2}$–4. Units: 10^{13} g s^{-1}

from the SH_1 theory in two significant ways: it is vertically asymmetric (with a strong recirculation aloft) and it extends to the jet core only for the high-range tropical flow (Fig. 2). The HH80 numerical solutions display a similar vertical asymmetry in flows with a low dissipation. The AXISYMMETRIC Ferrel cell is exceptionally strong because of the nonlinearity allowed by the moist inviscid atmosphere. This frictionally driven cell lies in the barotropic region and, in the high range, it interacts with the strong shear of the jet separation zone.

Elsewhere, the secondary cell pair occupy the baroclinic zone and try to make it less baroclinic, just as the primary cells make their barotropic zone more barotropic. The secondary Ferrel cell is detached from the surface and linked to the internal heat sink provided by the strong radiative cooling (Fig. 6a), in contrast to the PBL-bound, frictionally driven main Ferrel cell. Exceptions occur at $\Omega^* = 1$, where the secondary Hadley cell is weak and the Ferrel cells merge, and at $\Omega^* = 4$, where the secondary Ferrel cell vanishes. Eliassen's (1951) theory describes the cell maintenance in terms of the existing heat and momentum sources and sinks, but it does not explain the cell genesis and scale selection. The values of the conversion term $\langle P; K_\chi \rangle$ in Table 1 show that the main Hadley cell dominates at $\Omega^* = \frac{1}{2}$ and 2, that the main Ferrel cell prevails in the transitional state at

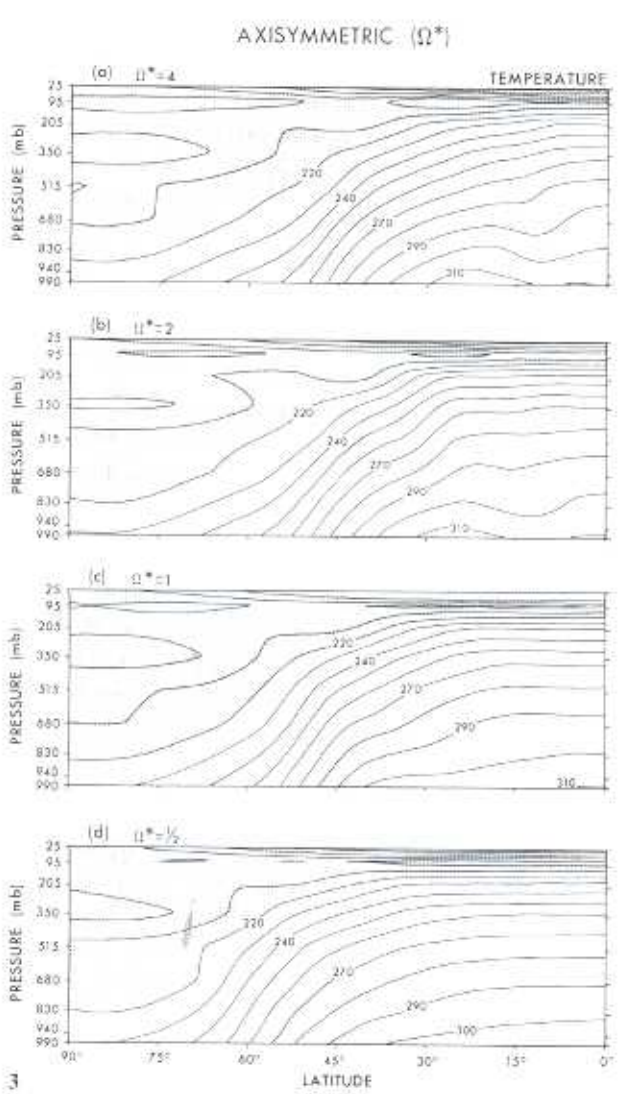

3

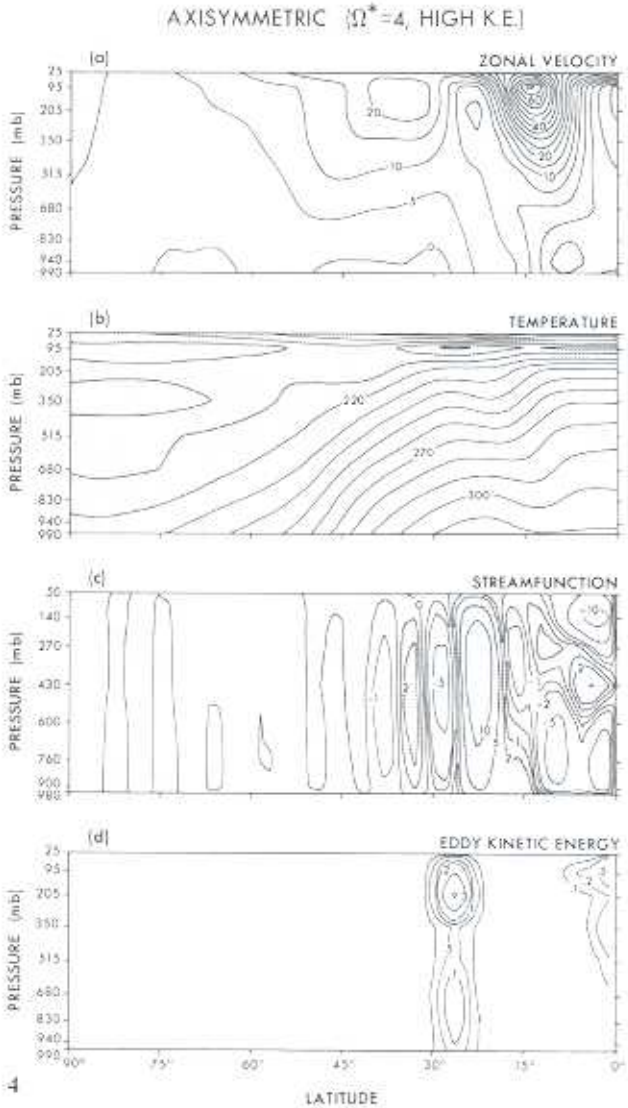

4

Fig. 3. Meridional distribution of the mean temperature for the AXISYMMETRIC model with $\Omega^* = \frac{1}{2}$–4. Units: K

Fig. 4. Meridional distribution of the mean zonal wind, temperature, stream function, eddy kinetic energy for the AXISYMMETRIC model with $\Omega^* = 4$, during the variant phase. Units: ms^{-1}, K, 10^{11} gs^{-1}, 10^{1} J kg^{-1}

$\Omega^* = 1$, and that the major cells are comparable at $\Omega^* = 4$. The main Ferrel cell is always strong, emphasizing just how important the higher-order meridional mode is for the moist inviscid atmosphere.

2.3 The AXISYMMETRIC(4) variant circulation (Fig. 4)

In its high-energy variant phase, the AXISYMMETRIC(4) circulation in Fig. 4 has most of its extra energy located in the tropical jet, which increases from 40 ms^{-1} to 70 ms^{-1} in amplitude, while being displaced 5° poleward by the deeper equatorial easterlies. With the development of the intervening easterlies, the two jets separate as completely as in the AXISYMMETRIC(2) case. The midlatitude jet remains essentially unaltered, however, and maintains a thermal wind balance poleward of its core at $\theta = 40°$. Related changes occur for the meridional flow in the tropics and the separation zone: the main Hadley cell widens below and weakens aloft; the main Ferrel cell becomes stronger but slimmer; and the secondary cells strengthen in the baroclinic zone (Fig. 4c). According to the conversion term $\{P:K_Z\}$ in Table 1, the Hadley cell really dominates in this circulation. Changes in the temperature field are limited to the tropical jet, where a second baroclinic front

forms in association with the stronger vertical shear and Hadley cell. The eddy kinetic energy produced by the shear instability and by the equatorial convection also increases in the AXISYMMETRIC(4) variant state (Fig. 4d).

We do not know why the AXISYMMETRIC(4) system fails to equilibrate simply, or why the variant state has this particular form. We can but repeat the argument made for the MOIST(8) variant state in § I-4.5: that the meridional circulation becomes more nonlinear, through terms such as $\nabla \cdot (vv)$, when Ω^* increases and confines the Hadley cell to the equatorial region. The effect occurs at $\Omega^* = 4$, rather than at $\Omega^* = 8$, because the AXISYMMETRIC circulations are generally more nonlinear than their MOIST counterparts. We expect deviations from the SH_1 theory to originate near the equator, and they do: only the tropical flow fails to equilibrate simply. No symmetric instabilities are apparent in this or any other AXISYMMETRIC circulation, being eliminated by the strong static stability set up by the moist convection.

2.4 The budgets and balances (Table 1, Figs. 5–7)

The global temperatures in Table 1 again all approach Earth's effective temperature despite major changes in the heat balance. According to the AXISYMMETRIC(1) case in Fig. 5, the advection and convection dominate the heat balance and generally match each other at rates that exceed the radiative cooling by a factor of 3 at all latitudes. Such intense dynamical exchanges occur only near the equator in the MOIST circulations. The meridional circulation is clearly not driven by a radiative-convective temperature field: the cells and the convection are too strongly coupled to be described by the SH_1 theory. Furthermore, the advection and convection extend to the pole, even though the atmosphere is in a radiative equilibrium in high latitudes (Fig. 6a). This shows that the high-order modes, unlike the SH_1 modes, penetrate beyond their source region. The radiation may still, however, determine the gross zonal flow and temperature, given that the advection and convection tend to compensate each other locally. In transporting the heat poleward, the AXISYMMETRIC(1) Hadley cell heats its central region and cools its edges; the Ferrel cell does the opposite.

According to the AXISYMMETRIC(1) momentum balance in Fig. 7, the cells alter the zonal flow significantly, despite the weakness of the surface momentum source, and help give the jet its three-part structure. The surface torques become strong when easterly tradewinds develop in the high range (Table 1). To produce such tradewinds, an atmosphere needs only a strong equatorward flow in the tropical PBL. This can be eddy induced, as in the MOIST unstable ranges, or diabatically driven, as in the AXISYMMETRIC high range and the OBLIQUE system. The subgrid mixing balances the residual of the momentum advection and the surface torque.

3 OBLIQUE(Ω^*,θ_p) circulations

To isolate the solstitial flow elements and to explore the parametric variability of oblique moist atmospheres, we evaluate a GCM with tilts ranging up to the 90° limit. Although the model is too idealized for climate studies, the OBLIQUE solutions indicate what seasonal extremes would occur, and what states Earth's atmosphere tends toward, in the absence of the restraint provided by the oceanic heat storage. The solutions also indicate how Mars' circulation might change as its obliquity varies from 15° to 35° over the millenia (see § 5.2).

The OBLIQUE model is based on the moist GCM described in § I-2. The solar insolation at the top of the atmosphere is still specified as a function of latitude, but is now based on a zenith angle that depends on a solar declination angle set permanently at the solstitial value θ_p. The radiation calculations then use the predicted water-vapor distribution and the annual-mean values (at $\Omega^* = 1$) of the carbon dioxide (a constant), the ozone (a function of latitude and height), and the cloud properties (in three layers). No problems occur in the frigid unlit winter hemispheres, where the radiative exchanges are due mainly to the carbon dioxide and a small amount of water vapor, but the accuracy is reduced in tropospheric regions cooler than 200 K because not all carbon-dioxide lines are represented at such temperatures. These limitations have no dynamical significance, but the OBLIQUE circulations are, like the MOIST flows, relatively forced by radiative exchanges that are partially tuned towards the annual-mean state at $\Omega^* = 1$.

The OBLIQUE(Ω^*,θ_p) set covers low, medium and high tilts by setting $\theta_p = 10°$, 25° and 90°, and ranges over medium and high rotation rates by setting $\Omega^* = ½$, 1, 2 and 4; see Table 2. The solutions for $\theta_p = 10°$ and 25° represent states in which the maximum surface temperature (T_s)

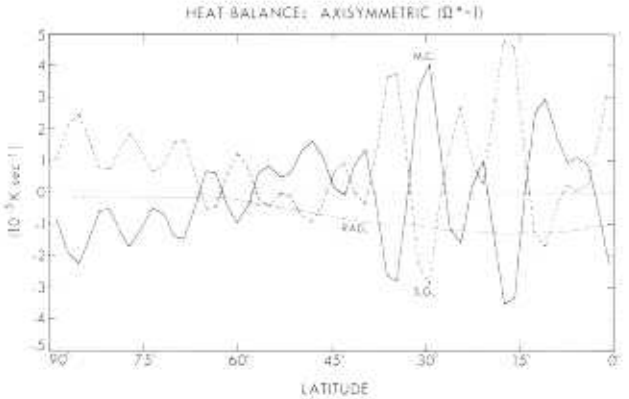

Fig. 5. Latitudinal distribution of the contributions to the mean rate of temperature change by the meridional circulation (*M.C.*), the eddies (*EDDY*), the radiation (*RAD*), the subgrid processes (*S.G.*) in the AXISYMMETRIC model with $\Omega^*=1$. Units: 10^{-5} K s^{-1}

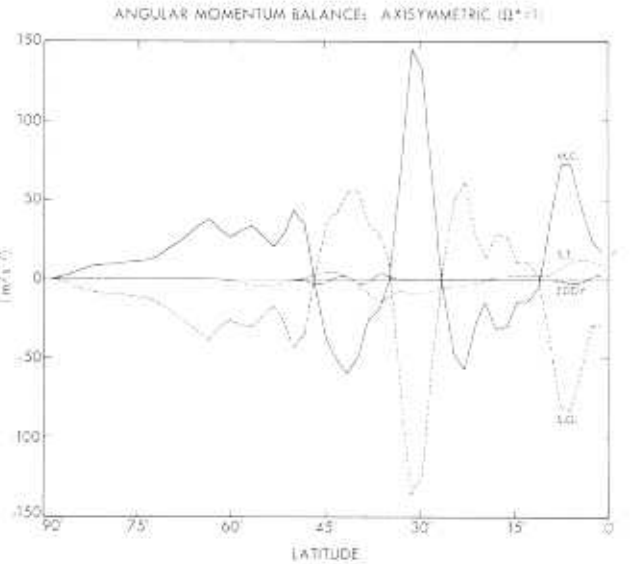

Fig. 7. Latitudinal distribution of the contributions to the mean rate of angular-momentum change by the meridional circulation (*M.C.*), the eddies (*EDDY*), the surface torque (*S.T.*), the subgrid diffusion (*S.G.*) in the AXISYMMETRIC model with $\Omega^*=1$. Units: m^2 s^{-2}

occurs in midlatitudes and high latitudes, respectively. The state with $\theta_P=25°$ is also typical of many planets (Williams 1985, Table 4). In the solstitial limit at $\theta_P=90°$, the sun shines directly and continuously over the pole and produces the peak T_s there. In such extreme cases, the area of maximum heating is much smaller than at equinox, so the surface becomes very hot and produces moisture amounts that cannot be handled by the standard GCM radiation code. Consequently, to keep temperatures below the critical 320-K level, the solar constant is reduced to ¾ and ½ its normal value when $\theta_P=25°$ and 90°, respectively. On the other hand, during equinox ($\theta_P=0°$) the surface temperature peaks at or near the equator, a

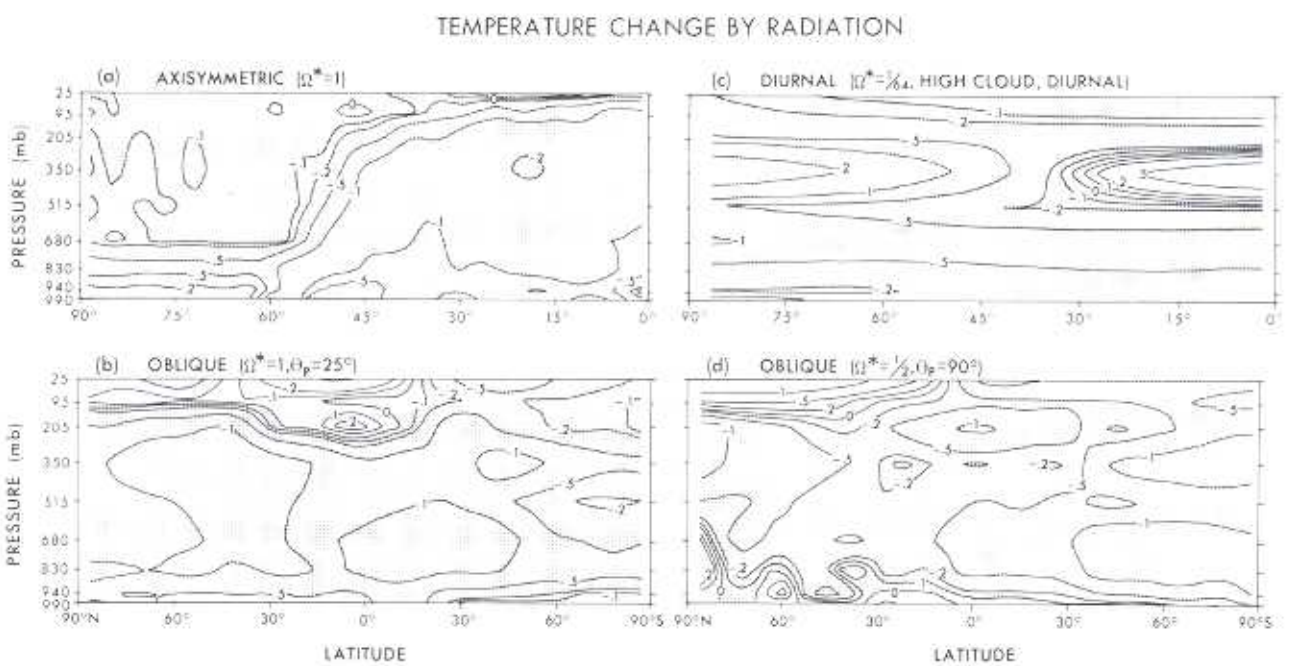

Fig. 6. Meridional distribution of the mean rate of temperature change due to radiation, for representative cases from various sets. Units: 10^{-5} K s^{-1}

Table 2. OBLIQUE circulations: energy, heat and momentum integrals

Case				Energy					Heat					Momentum				
Ω^a	θ_p	sc	τ_f	K_Z	K_E	$P:K_Z$	$P:K_E$	$K_Z:K_E$	T^b	$\bar{r}^b$	RAD	$v'T'^{c,d}$	$-\omega'T'$	Max[c] torque	$v'M'^{c,d}$	$-\omega'M'$	Max[c] $\lvert u\rvert$	Max $\lvert v\rvert$
4	10°	1	600	45	59	111	167	13	256.3	5.6	− 999	−331	335	112	− 30	−48	38	3.3
2	10°	1	450	79	75	188	200	23	256.6	4.9	−1017	−350	455	87	8	− 1	58	4.0
1	10°	1	400	162	79	130	259	− 47	256.3	4.5	−1026	−380	531	− 81	− 65	256	90	5.8
½	10°	1	400	280	82	242	181	− 7	255.9	4.0	−1031	−269	428	− 55	132	215	104	7.9
4	25°	¾	550	86	54	168	239	2	234.4	2.6	− 690	−554	570	−153	− 95	237	70	4.1
2	25°	¾	550	212	82	171	315	− 41	235.0	1.8	− 716	−476	701	125	−116	277	84	5.2
1	25°	¾	650	399	90	220	301	− 77	234.6	1.2	− 720	−462	683	−118	− 29	265	123	7.8
½	25°	¾	450	462	84	293	173	80	233.8	0.8	− 690	−276	502	− 97	343	213	106	10.2
4[e]	90°	5/12	900	563	77	206	416	−138	190.2	0.5	− 408	−487	974	−121	39	84	140	2.6
2	90°	5/12	750	897	106	288	429	12	195.3	0.1	− 413	−509	977	106	232	231	152	4.3
1	90°	½	700	543	136	400	518	14	210.3	0.0	− 547	−660	1151	−149	485	124	182	7.3
½	90°	½	900	2990	79	624	100	121	210.8	0.0	− 474	−134	371	−132	− 61	358	207	9.0
Units			Days	J kg^{-1}		10^{-6} W kg^{-1}			K	cm water	10^{-8} Ks^{-1}	10^{1} J m kg^{-1} s^{-1}	10^{-2} W m^{-2}	m^2 s^{-2}	10^{3} kg^2 m^{-2} s^{-2}	10^{2}	m s^{-1}	

[a] Extended with R42 resolution
[b] Instantaneous values
[c] Local values
[d] Symbolic notation for eddy integrals

τ_f denotes integration period. Resolution B used in all cases; see Table 1 of Part I
sc denotes factor by which solar constant is modified
RAD denotes radiative heating rate

state that is reasonably represented by the MOIST solutions of § I-4.

For computational economy, an R15 resolution and a 120° crescent domain are used for the integrations (see Table I-1). Although this resolution cannot describe the small high-range eddies accurately, the solutions do give an adequate indication of the various flows — as is verified by an R42 calculation for the OBLIQUE(4,90°) case. In the presentation, we group the solutions by their obliquity, because θ_P has a greater influence than Ω^* on the circulation variability in the solstitial regime. But first we must discuss theories for the solstitial Hadley state and the unstable easterly jet.

3.1 Solstitial circulation dynamics

Allowing heating asymmetries about the equator introduces new dynamical modes. These modes can be interpreted in terms of standard Hadley and quasi-geostrophic theories if we first define the solstitial-symmetric-Hadley (SSH) state, with its summer easterly and winter westerly jets, and if we then define the QG-Hadley and QG_γ elements that describe the natural forms of these jets.

The solstitial-symmetric-Hadley (SSH) circulation (Fig. 8). In Part I, we briefly described the HH80 theory for the symmetric-Hadley circulations driven by a heating that peaks, and is symmetric about, the equator. Such equinoctial flows contain a momentum wind u_M and a Hadley cell in lower latitudes, and a radiative-equilibrium thermal wind u_E in higher latitudes. The cell extends from the equator to the latitude θ_H where the two winds meet to form a jet. This first-order SH_1 theory is useful for understanding the NH and QH elements that arise in the MOIST and DRY solutions, but it has limitations, as the AXISYMMETRIC solutions in § 2 show. To help describe and explain the OBLIQUE solutions, we now modify the HH80 geometric argument to define the axisymmetric circulations driven by a solstitial heating having a strong asymmetry about the equator.

The SSH mode is best defined for the limiting solstitial state in which the heating is strongest at the summer (north) pole and weakest at the winter pole. Systems with a moderate seasonal variation then lie between the equinoctial (SH) and solstitial (SSH) limiting states. The OBLIQUE solutions show that the SH_1 state exists for atmospheres with only a weak heating asymmetry, whereas the SSH state prevails over a wide range

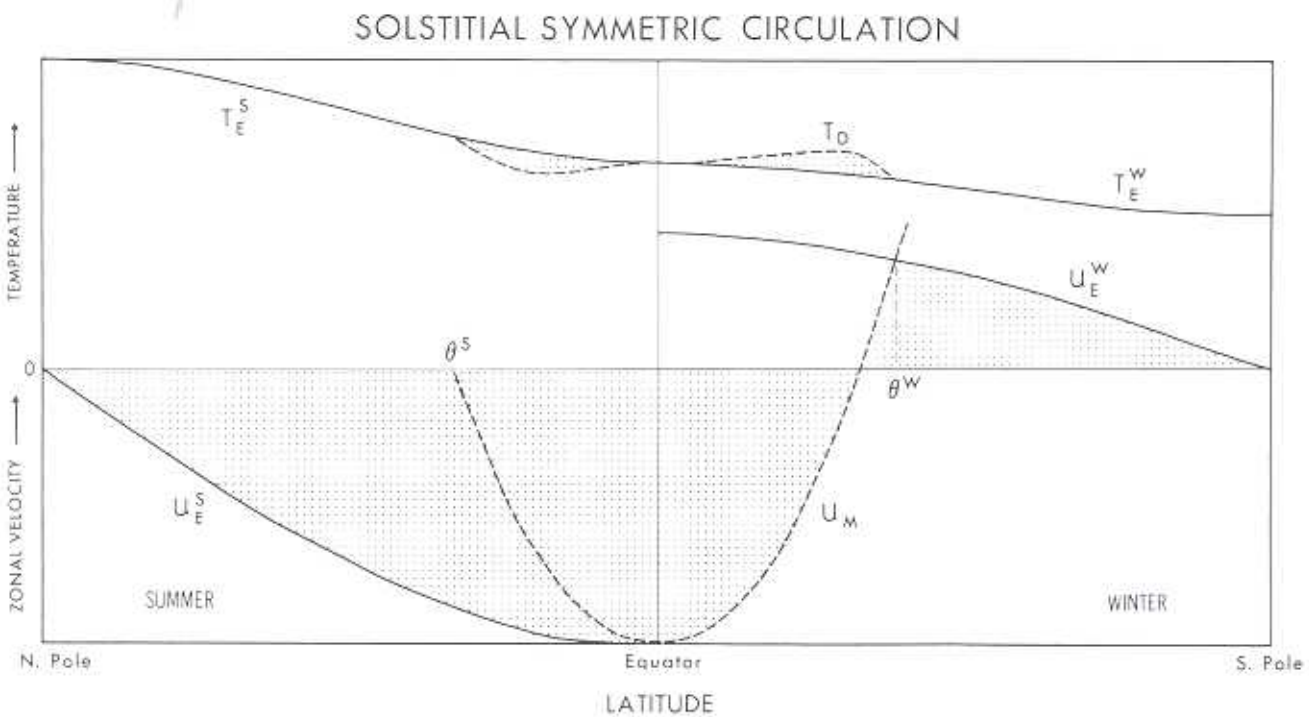

Fig. 8. Schematic illustration of the interplay between the thermal winds u_E^S and u_E^W of the summer and winter hemispheres and the momentum-conserving wind u_M in axisymmetric circulations during solstice. *Shading* indicates resulting zonal wind

of obliquities (for $\theta_p \geq 10°$). The simplicity of the solstitial limit makes it easy to modify the geometric argument, but no rigorous theory is developed.

To represent the pole-to-pole baroclinicity, we write the vertically averaged radiative temperature in the HH80 form

$$\frac{T_E}{T_0} = 1 - \frac{2}{3}\Delta_H P_2(\sin\theta) \tag{1}$$

where T_0 is the hemispheric mean temperature, Δ_H the nondimensional hemispheric baroclinicity, and $P_2(y) = (3y^2 - 1)/2$ the second Legendre polynomial. For plotting the temperature profile in Fig. 8, we set $\Delta_H^W = \frac{1}{2}|\Delta_H^S|$, where the summer baroclinicity Δ_H^S is negative and the winter baroclinicity Δ_H^W is positive. This temperature field produces an easterly thermal wind $u_E^S = -a\Omega R_E^S \cos\theta$ at the summer tropopause and a westerly thermal wind $u_E^W = a\Omega R_E^W \cos\theta$ at the winter tropopause; where $R_E^S = gH|\Delta_H^S|/(a\Omega)^2$ and $R_E^W = gH\Delta_H^W/(a\Omega)^2$ are the hemispheric Rossby numbers for a Boussinesq atmosphere of depth H.

The summer thermal wind, being easterly, does not violate the constraint that the angular momentum not exceed $a^2\Omega$ — see HH80 for details. If such thermal winds occurred in both hemispheres, they would represent the simplest solution to the full equations. But this requires that both poles be hotter than the equator — an unlikely configuration. The winter thermal wind, on the other hand, cannot be valid in low latitudes because it does violate the angular-momentum constraint in that region. Consequently, a momentum wind must exist in the winter tropics to eliminate the discontinuity between the two thermal winds, and to replace the invalid u_E^W wind in the winter tropics. Given that a u_E^S wind can exist as a first approximation, it seems reasonable to assume that its equatorial value provides the boundary value for the momentum wind. The shaded region in Fig. 8 depicts the net zonal flow that forms from the interplay of the three winds. The momentum wind $u_M = a\Omega(\sin^2\theta - R_E^S)/\cos\theta$ extends from the equator to the latitude where it intersects the u_E^W wind, to θ^W.

The vertical shear created between the momentum and surface winds produces, through the thermal wind balance, a dynamic temperature T_D that increases more slowly northward than T_E in Fig. 8. The Hadley cell associated with T_D conserves heat by warming the winter tropics and cooling the summer tropics, in such a way that the shaded areas between T_E and T_D cancel. The cell extends from θ^S to θ^W, where $\theta^S \simeq |\theta^W| \simeq (R_E^S)^{1/2}$, and so has nearly the same latitudinal range as the SH_1 cell pair. It produces westerly and easterly tradewinds in the summer and winter tropics, respectively.

Thus the summer thermal wind u_E^S drives the winter momentum wind u_M that bounds the winter thermal wind u_E^W, while inducing a dynamic temperature T_D and a Hadley cell that transports heat southward. The u_E^S wind then responds to the T_D field by moving its peak from the equator, thereby altering the value that initializes the u_M wind and changing the temperature and cell, and so on until equilibration. In this view, the summer hemisphere is clearly in charge of the circulation, as might be expected from its being the energy source. The extreme case in which the winter hemisphere is completely unlit, so that Δ_H^W and u_E^W vanish, occurs as a natural limit of the theory.

This SSH theory differs fundamentally from the SH_1 theory in the way the momentum wind is initialized. In the SH_1 case, the momentum wind is set to zero at the latitude where the cell upflow communicates the value of the surface momentum to the atmosphere. But in the SSH case the cell upflow occurs in the u_E^S wind, so the momentum wind cannot be initialized by surface values. Given these differences in the geometric argument, the SSH ideas remain tentative.

The QG-Hadley (QGH) circulation element. The OBLIQUE mean flows resemble the axisymmetric flows described by the SSH theory, and consist of a cross-equatorial Hadley cell and four solstitial winds: an easterly jet and a westerly tradewind in the summer hemisphere, and a westerly jet and an easterly tradewind in the winter hemisphere (see Fig. 10g). The easterly jet switches from a thermal wind to a momentum wind as it extends across the equator into the winter tropics, where it then merges with the easterly tradewinds. To define the dynamics of the unstable easterly jet, we isolate the invariant features of the OBLIQUE states and form the idealized QG-Hadley (QGH) element in Fig. 9 whose mean flow is governed mainly by Hadley processes, and whose eddies are governed mainly by quasi-geostrophic dynamics.

The QGH eddies in Fig. 9 produce a downgradient (equatorward) heat flux at low levels, release potential energy at midlevels ($\{P:K_E\} > 0$), and reduce the zonal flow aloft ($\{K_Z:K_E\} > 0$), all in the manner expected of an easterly instability. Note that the negative baroclinicity reverses the sign of the correlation between the latitudinal and

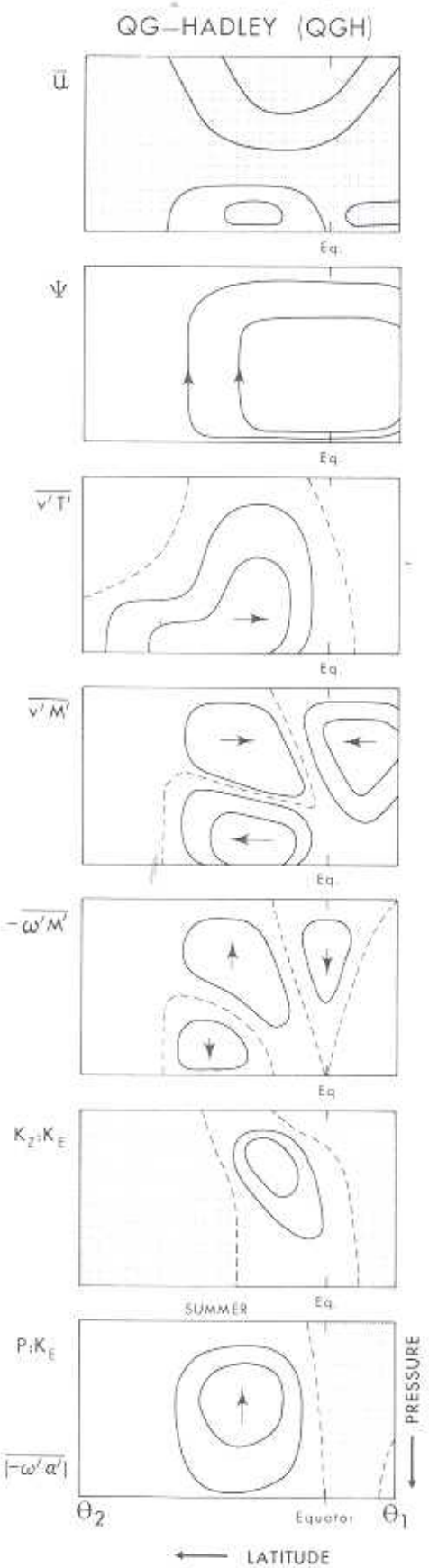

vertical fluxes, in agreement with the quasi-geostrophic wave relation $w/v = -z\Theta_y/\Theta_z$ (Gill 1982, § 13.2). On the other hand, the vertically bimodal eddy momentum fluxes — convergent aloft and northward-traversing below — are unique to the QGH element, but their cause remains uncertain.

Only the cause of the eddy momentum transport ($v'M'$) in the winter tropics is clear: the northward flux arises from waves dispersing south from the easterly instability and north from the westerly instability. The winter westerly otherwise behaves like a QG_y element, with its eddies transporting momentum toward the south pole — see § I-3.2. But in the summer hemisphere the transports in the tropics cannot be so accurately related to the waves and instabilities because no eddy cycle has been evaluated for an easterly jet that co-exists with a Hadley cell. Nevertheless, the upper-level fluxes do appear to be consistent with the action of an internal instability, and the lower-level flux appears to be consistent with a southward wave dispersion, according to the following linear theories.

Consider first the momentum fluxes produced by linear *internal* instabilities in a two-layer fluid. At the quasi-geostrophic, β-plane order, they are described by the expression

$$[(v'M')_1 + (v'M')_2]_y = \frac{k}{2} c_i \left[\frac{|\hat{q}_1|^2}{\bar{q}_{1y}} + \frac{|\hat{q}_2|^2}{\bar{q}_{2y}} \right] e^{2kc_i t} \quad (2)$$

for baroclinic waves of the form $\hat{q}\exp[ik(x-ct)]$ — see Held (1975) for details. For an internal instability to occur, the potential vorticity gradient $\bar{q}_y$ must change sign somewhere. In westerly jets, we have $\bar{q}_{1y} > 0$ everywhere aloft but $\bar{q}_{2y} < 0$ in the center below, leading to a net flux of westerly momentum into the low-level flow. In easterly jets, we have $\bar{q}_{2y} > 0$ everywhere below (because $\bar{u}_2$ is weak) but $\bar{q}_{1y} < 0$ in the center aloft (because both shears oppose β), leading to a flux into the jet core (cf. Pfister 1985). Thus linear internal instabilities converge momentum into both westerly and easterly jets — but at different heights — to boost the former and reduce the latter. The QGH element can be regarded as having such a converging flux aloft if the cross-equatorial component is included. The lower-level flux, however,

Fig. 9. Schematic summary of the quasi-geostrophic-Hadley circulation element that occurs in low summer latitudes during solstice ($\theta_0 \geq 10°$) for the Ω^* mid and high ranges. See Fig. I-1 for notation

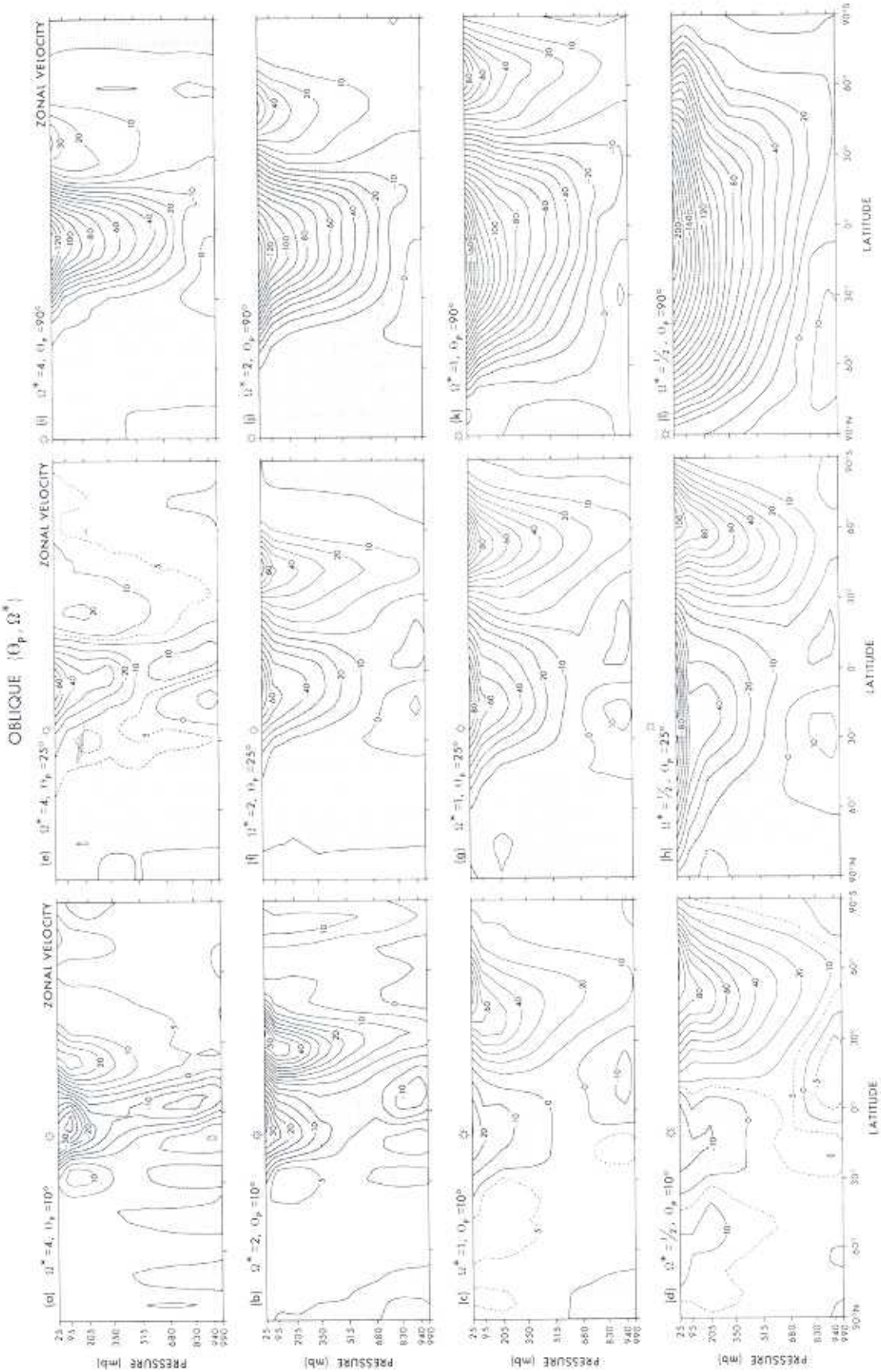

Fig. 10. Meridional distribution of the mean zonal wind for the OBLIQUE model with $\Omega^* = \frac{1}{2}$, 4 and $\theta_p = 10°$, 25°, 90°. Units: ms^{-1}

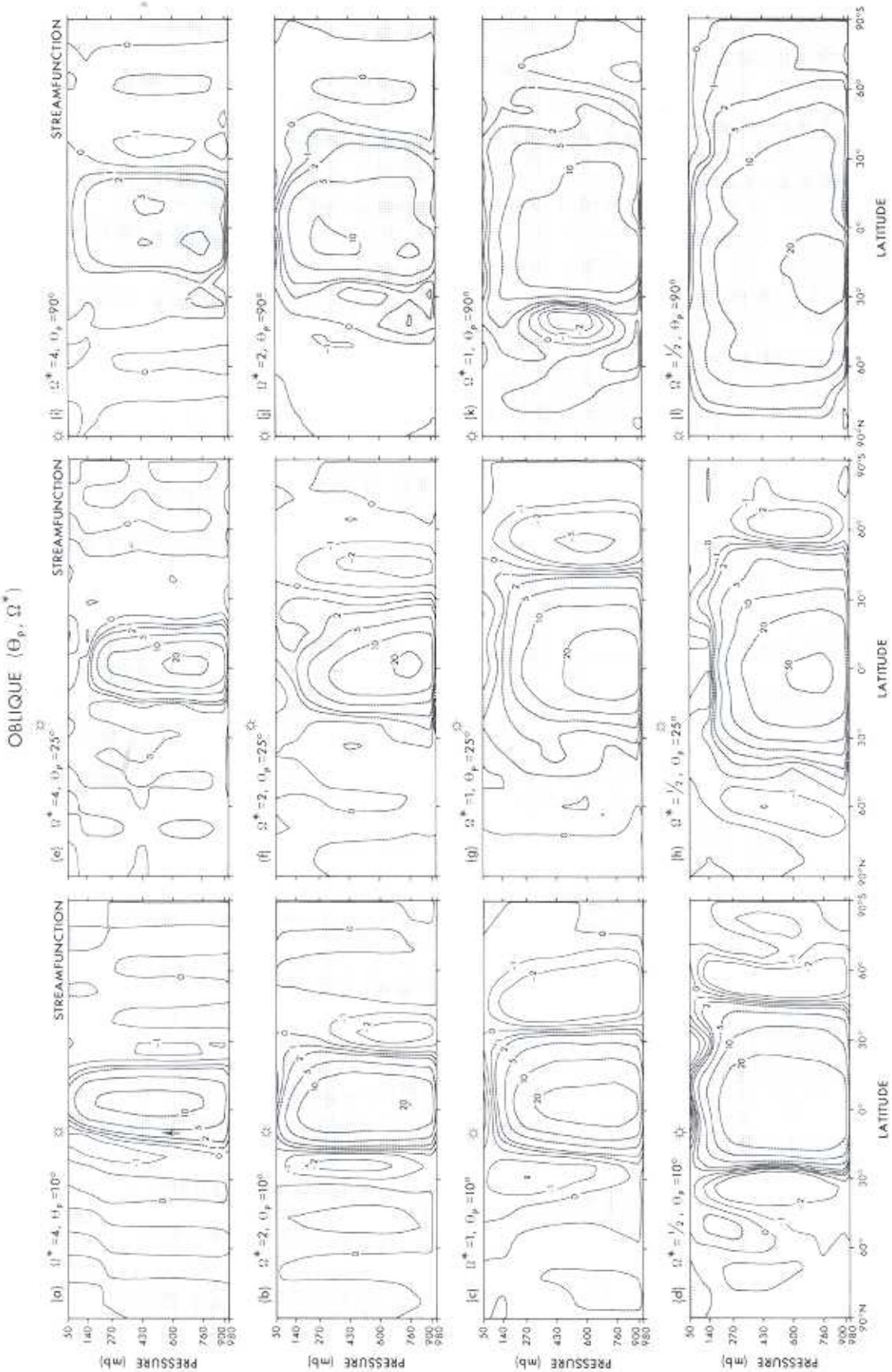

Fig. 11. Meridional distribution of the mean stream function for the OBLIQUE model with $\Omega^*=\frac{1}{2}$-4 and $\Theta_p=10°$-90°. Units: 10^{13} g s^{-1}

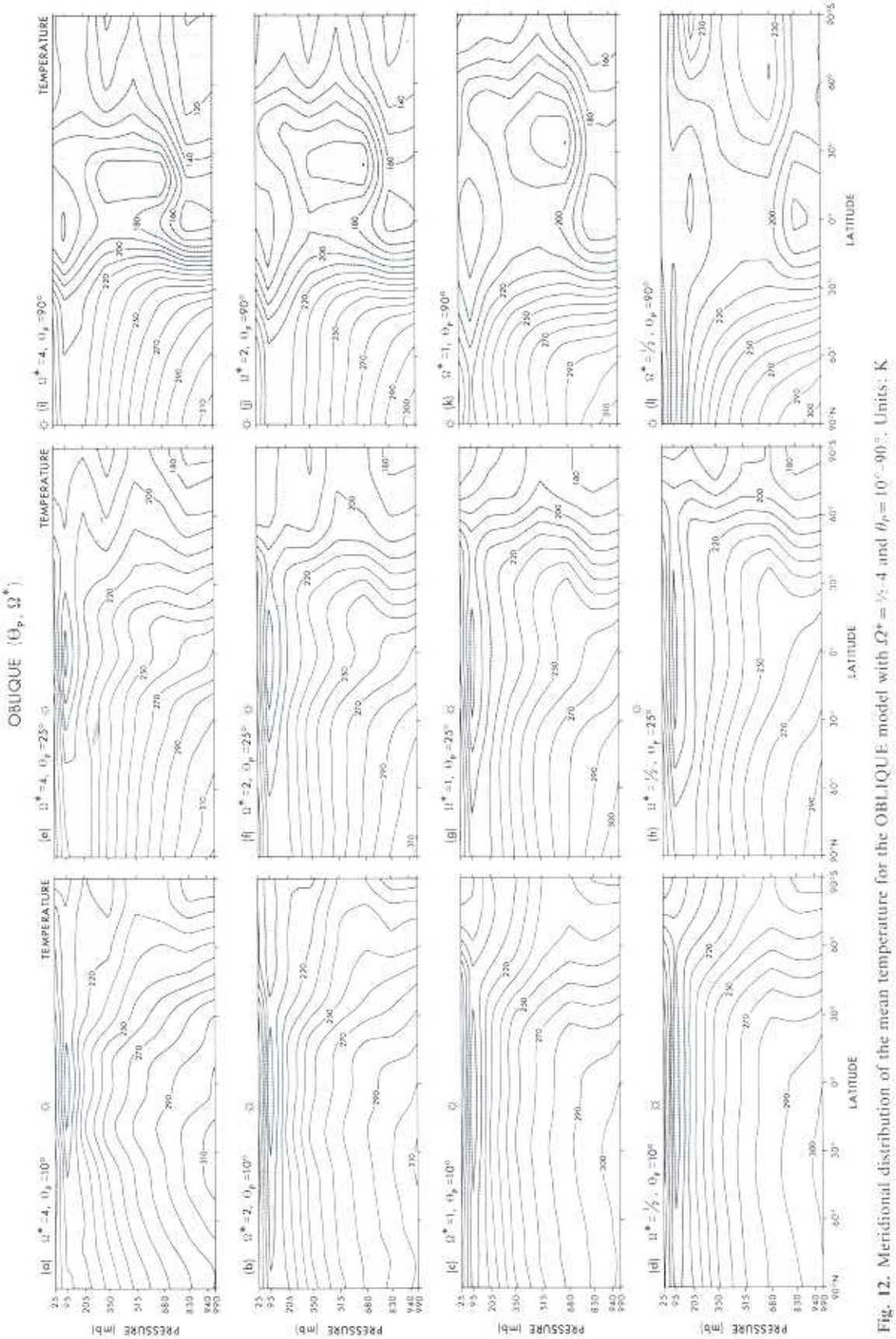

Fig. 12. Meridional distribution of the mean temperature for the OBLIQUE model with $\Omega^* = \frac{1}{2}$-4 and $\Theta_p = 10°$-90°. Units: K

cannot arise directly from a linear internal instability. Both westerly and easterly instabilities induce a meridional circulation that has an indirect cell at the center and direct cells at the edges (Phillips 1954), but such flows would be submerged by the Hadley cell in the QGH element.

Consider next the momentum fluxes produced by linear *surface* instabilities in a continuous fluid. At the quasi-geostrophic, β-plane order, they are described by the expression

$$(\overline{v'M'})_s = kc_i \left[\int_0^H \frac{|\hat{q}|^2}{\bar{q}_y} dz + \frac{f_0^2}{N^2} \frac{|\hat{\psi}_z|^2}{\bar{u}_z} \Big|_0^H \right] e^{2kc_i t} \quad (3)$$

where the double bar denotes averaging over longitude and height. From the second term on the right, we see that an easterly shear produces a northward flux near the surface and a southward flux near the tropopause. Although the QGH fluxes do have such a vertically bimodal form in the subtropics, their latitudinal variation can be explained only by including the internal $\bar{q}_y$ factor. The Hadley cell complicates the instability and its fluxes by reversing the vertical shear near the surface.

Planetary wave dispersion, however, is known to be more important than the instability in shaping the momentum fluxes of the QG_y westerlies, and the eddy geopotential fluxes in Fig. 17b and d show that waves are also active in the QGH element, propagating energy southward across the equator near the surface and in the stratosphere. Such waves tend to produce a northward momentum flux, so could account for all of the lower-level flux and for modifications to the upper-level fluxes. Theory tells us that linear waves can propagate in easterly currents with a negative $\bar{q}_y$, according to the refractive index $m^2 = N^2 f_0^{-2} [\bar{q}_y (\bar{u} - c)^{-1} - (k^2 + l^2)]$, and in regions where the Hadley cell has a poleward flow (aloft in the winter tropics, below in the summer tropics), according to Schneider and Watterson (1984). Consequently, the planetary waves can easily contribute to the QGH fluxes.

Thus, we tentatively conclude that the upper-level converging fluxes in the QGH element are due primarily to an internal instability (with some modification by the southward-dispersing waves), and that the lower-level northward flux is due primarily to southward-dispersing waves (with some modification by a surface instability). The idealized QGH momentum flux is best seen in those OBLIQUE solutions where the easterly and westerly jets have comparable instabilities and waves, at $\theta_P = 25°$ (Fig. 16g). Otherwise, the flux in the winter tropics is driven mainly by waves emanating from the westerly instability when $\theta_P = 10°$, and from the easterly instability when $\theta_P = 90°$. The OBLIQUE fluxes vary substantially with the parameters, with changes being attributable to variations in $\bar{q}_y$ and $\bar{u}_z$.

3.2 *The OBLIQUE(Ω^*, θ_P) solutions*

Having defined the solstitial elements, we can now describe the basic character and the parametric variability of the OBLIQUE mean fields and eddy fluxes.

The mean fields (Figs. 10–12). Solstitial circulations, as represented by the OBLIQUE(1,25°) solution in Figs. 10g–12g, are made up of four zonal winds and two meridional cells: an easterly QGH jet in the summer hemisphere and winter tropics, a westerly QG_y jet in the winter midlatitudes, easterly and westerly tradewinds in the winter and summer tropics, an equator-straddling Hadley cell, and a Ferrel cell in the winter midlatitudes. The Hadley cell extends more into the winter hemisphere than the summer hemisphere and associates with the easterly jet, the equatorward half of the westerly jet, and the two tradewinds — as in the SSH theory. The eddy-induced Ferrel cell lies at the core of the westerly jet — as in the QG_y theory. The temperature field has a pole-to-pole gradient, with a moderate negative summer baroclinicity and a strong winter baroclinicity, as well as a strong inversion and a vanishing tropopause toward the winter pole.

Solstitial circulations occur when the planet has a medium or high tilt ($\theta_P \geq 25°$). When it has a low tilt ($\theta_P = 10°$), the circulations have a mix of solstitial and equinoctial features in the summer hemisphere: a tropical easterly jet and a midlatitude westerly jet (Figs. 10c–12c). Multiple jets, such as occur in the MOIST high range, arise only when the tilt is low and the rotation high; but they are weak in Fig. 10a, b because of the low resolution.

The parameters θ_P and Ω^* control the scale but not the form of the solstitial states. The easterly jet and the Hadley cell in Figs. 10 and 11 widen as θ_P increases (because the baroclinicity intensifies) and narrow as Ω^* increases, in keeping with the theoretical relation $\theta_H \sim R_E^{1/2}$. The amplitude of the easterly jet, however, varies only

Fig. 13. Meridional distribution of the mean eddy kinetic energy for the OBLIQUE model with $\Omega^* = \frac{1}{2}, 1, 2$ and 4 and $\Theta_p = 10°, 25°, 90°$. Units: 10^1 J kg^{-1}

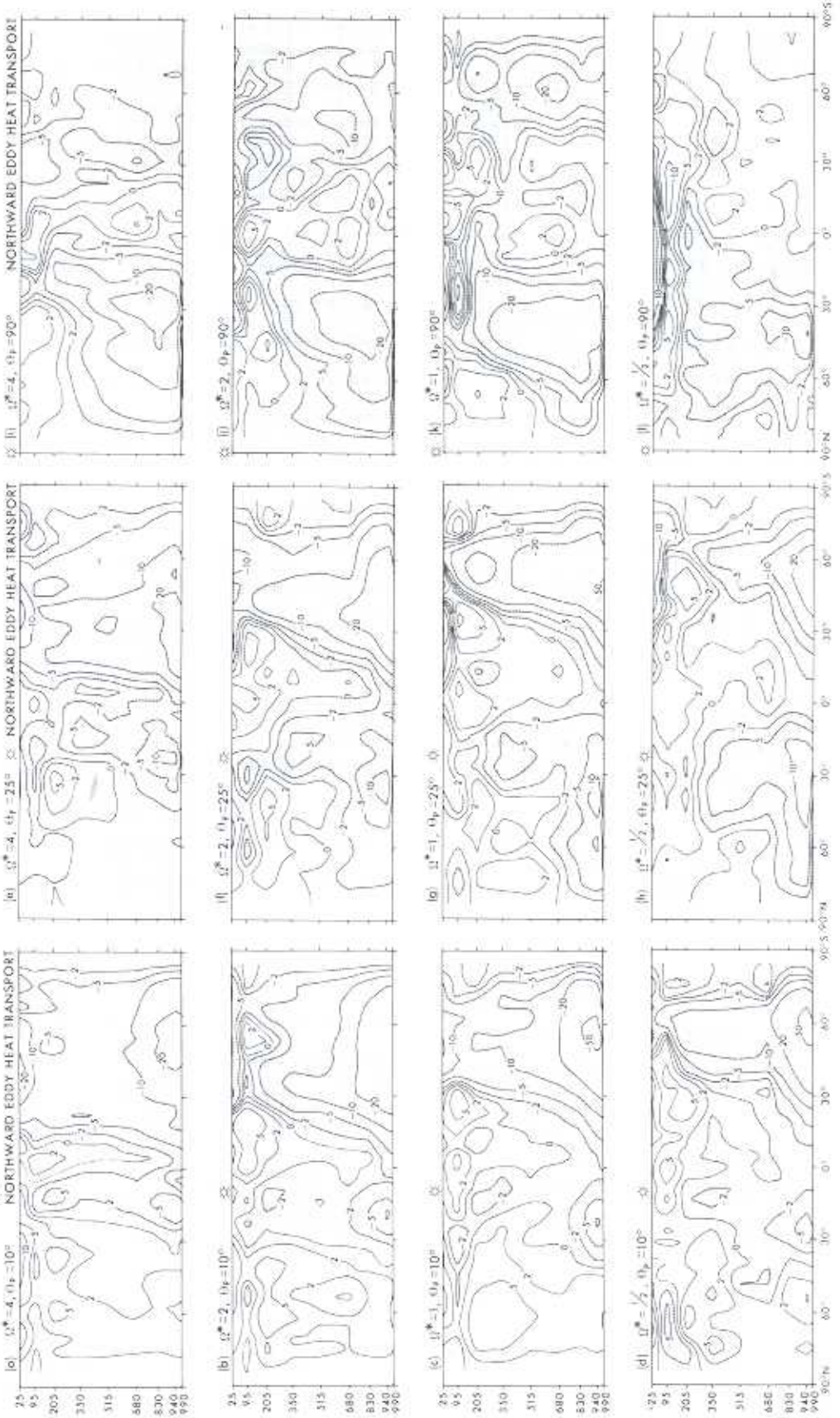

Fig. 14. Meridional distribution of the mean northward transport of heat by the eddies in the OBLIQUE model with $\Omega^* = \frac{1}{2}$–4 and $\theta_p = 10°$–90°. Units: 10^3 J m kg^{-1} s^{-1}

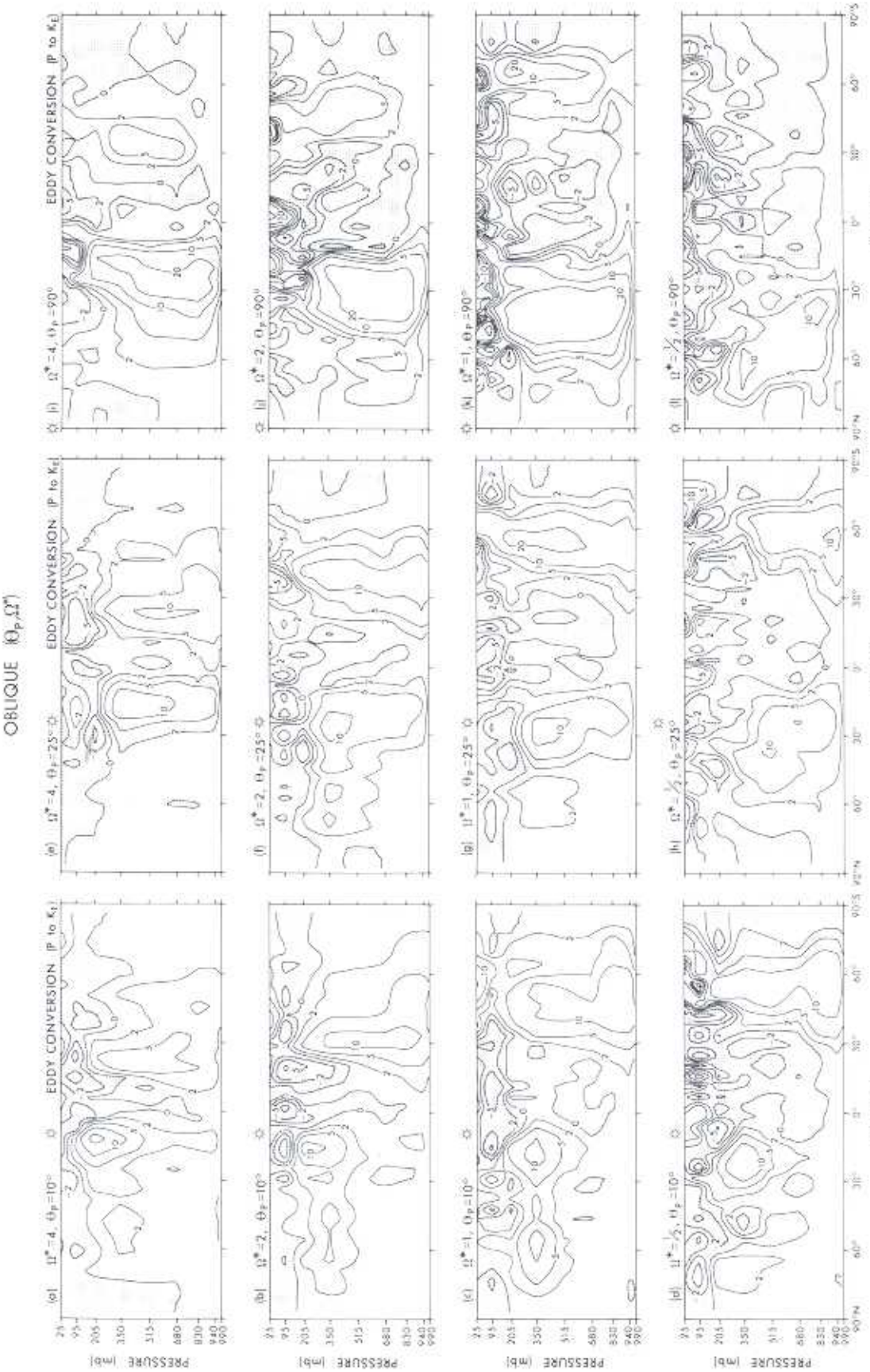

Fig. 15. Meridional distribution of the mean baroclinic energy conversion by the eddies in the OBLIQUE model with $\Omega^*=\frac{1}{2}$–4 and $\theta_p=10°$–90°. Units: 10^{-4} W kg^{-1}

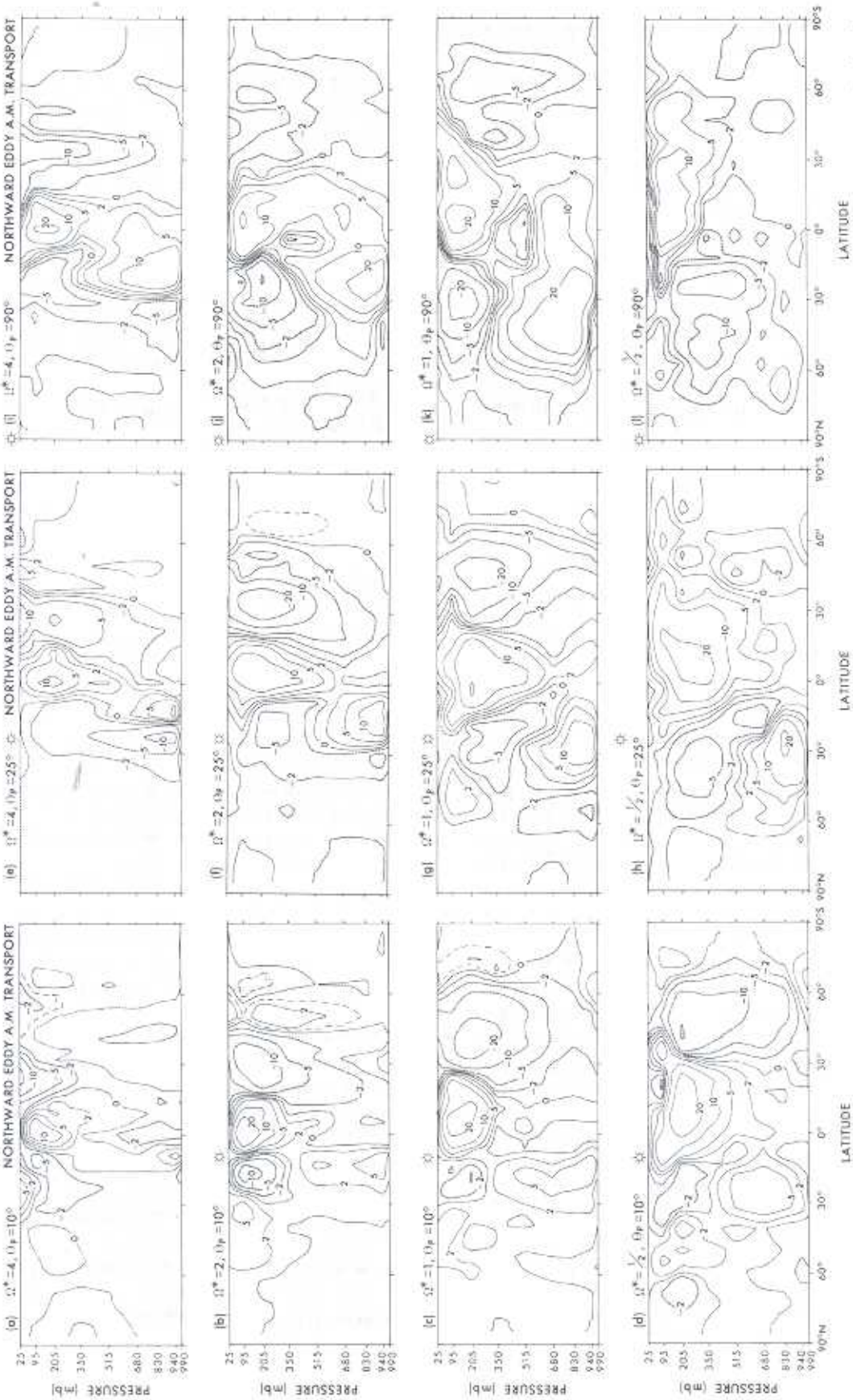

Fig. 16. Meridional distribution of the mean northward transport of angular momentum by the eddies in the OBLIQUE model with $\Omega^* = \frac{1}{2}$–4 and $\theta_p = 10°$–90°. Units: 10^7 m^3 s^{-2}

weakly with Ω^* because of compensating changes in the baroclinicity. Meanwhile in the winter hemisphere, the westerly jet and the Ferrel cell have widths and amplitudes that depend mainly on Ω^* through the eddy-scale L_R, when sufficient space exists for their full development. All jets move equatorward as Ω^* increases. The Hadley cell is moist and sharp for low tilts, but dry and diffuse for medium and high tilts.

The temperature field, of course, depends mainly on θ_p, with the summer baroclinicity becoming stronger and the winter inversion becoming hemispheric as the obliquity increases (Fig. 12). When the sun lies right over the north pole, the summer hemisphere develops an intense negative baroclinicity ($\Delta T_s \sim -130$ K), and the winter hemisphere develops a powerful inversion centered on a midtropospheric warm (220 K) hole (cf. Hunt 1982). The inversion arises from adiabatic heating in the Hadley cell's downflow, and moves equatorward as the cell narrows with increasing Ω^*. The tropopause forms only in the summer hemisphere.

An exceptional solstitial state, in which the easterly jet becomes global and the Hadley cell extends from pole to pole, occurs for the OBLIQUE(½,90°) configuration (Figs. 10l–11l). In this case, the inversion places its warm hole right at the winter pole, making it 40 K warmer than the summer pole aloft (Fig. 12l). The creation of the warm winter pole provides a powerful demonstration of the role of dynamics in shaping the temperature distribution.

The dynamics of the OBLIQUE(½,90°) jet differs from one hemisphere to the other: the easterly jet has a thermal-wind balance in the summer hemisphere but a momentum-wind balance in the winter hemisphere. Consequently, baroclinic instability occurs only in the summer hemisphere, and wave dispersion occurs only in the winter hemisphere. The easterly jet peaks right at the equator with a value (-207 ms^{-1}) that may be close to the maximum possible in this system. (Note that $a\Omega = 230$ ms^{-1} and $R_L = 1$ in this case.) Near the surface, each tradewind extends over a hemisphere, so global transports are needed to balance the torques. The global cell has a tight moist upflow over $\theta = (60°\text{–}90°)$N and a broad dry descent over $\theta = (30°\text{–}90°)$S (Fig. 11l).

At medium tilts, changes in the amplitudes of the instabilities cause a summer Ferrel cell to emerge in the OBLIQUE(½,25°) case, and the winter Ferrel cell to disappear in the OBLIQUE(4,25°) case (Fig. 11h,e). The OBLIQUE(1,25°) Hadley cell rises near 25°N and descends near 35°S, and is clearly unrelated to the thermal "equator" — which now lies at the summer pole. In these cases, the baroclinicity is strong in both hemispheres: ΔT_s goes from -35 K in summer to 90 K in winter.

At low tilts, the OBLIQUE(Ω^*,10°) surface temperatures peak further from the equator than Earth's atmosphere does during its summer solstice — because the GCM lacks an ocean heat storage to reduce the seasonal variation. Earth, in fact, corresponds to a GCM with an obliquity lying between 5° and 10°. (Note, however, that even when there is almost no radiative gradient in Earth's summer hemisphere, motions can be driven by the temperature gradients built up in the ocean over a succession of winters.) The OBLIQUE(1,10°) atmosphere has a low summer baroclinicity ($\Delta T_s \sim 5$ K), a strong winter baroclinicity ($\Delta T_s \sim 80$ K), and zonal and meridional flows that closely resemble Earth's in January or July (Manabe and Mahlman 1976, Fig. 4.1). The solstitial tradewinds are strong (± 10 ms^{-1}) and closely related to the diabatically driven Hadley cell, in contrast to the MOIST set where the tradewinds are produced by eddy-induced contributions to the meridional circulation. The westerly tradewinds, however, barely arise on Earth but are clearly present on Mars (Leovy 1985, Fig. 2).

The eddy fields (Figs. 13–17). The strongest kinetic energies produced by the solstitial eddies occur in the cores of the easterly and westerly jets, in association with the baroclinic instabilities (Fig. 13). The peak energy generally occurs in the westerly jet but switches to the easterly jet when that flow becomes predominant at $\theta_p = 90°$. The easterly tradewinds have the weakest eddies. The moist convection is confined to the summer high latitudes and contributes little to the generation of the eddy energy. In the exceptional OBLIQUE (½,90°) case in Fig. 13l, the eddies arise in the unstable summer easterly and propagate aloft into the stable winter easterly, according to the eddy geopotential flux ($v'\Phi'$).

The strong southward heat fluxes in the easterly and westerly jets in Fig. 14 are typical of baroclinic instabilities having a strong surface shear; while the weak northward fluxes in the upper-level tropics are typical of propagating planetary waves. The vertical heat fluxes in Fig. 15 show that all instabilities are located in the jet cores, with those in the westerly extending to the top of the atmosphere because no tropopause exists in the winter hemisphere. In the high-tilt systems, the heat fluxes fill most of the summer hemis-

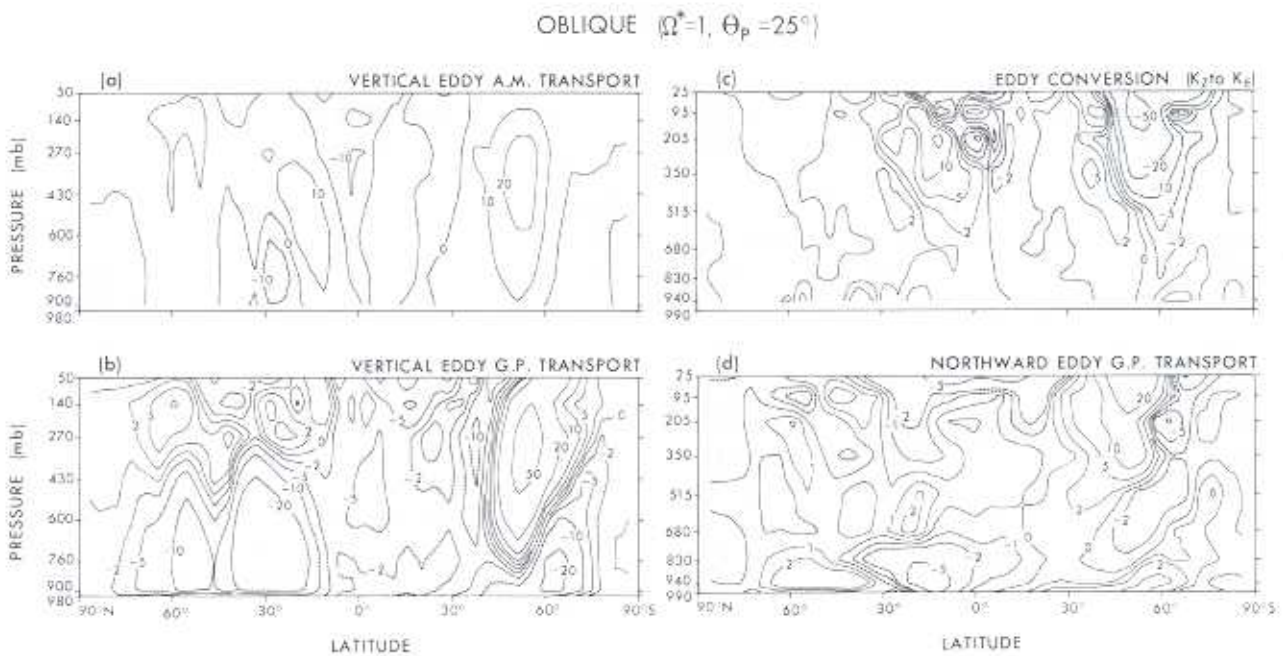

Fig. 17. Meridional distribution of the mean vertical angular-momentum transport, vertical geopotential transport, baroclinic energy conversion, and northward geopotential transport — all by the eddies in the OBLIQUE model with $\Omega^* = 1$, $\theta_p = 25°$. Units: 10^1 kg s^{-2}, 10^{-1} W m^{-2}, 10^{-4} W kg^{-1}, 10^2 J m kg^{-1} s^{-1}

phere because the easterly instability is so strong; whereas in the exceptional OBLIQUE(½, 90°) case, the winter heat flux vanishes because the winter easterly is so stable. On the other hand, the low-tilt flows have extra heat fluxes that show the summer westerly as having an internal form of instability.

The eddy momentum fluxes for the easterly jets, in Figs. 16, 17a, are all close to the idealized, vertically bimodal QGH form. Aloft, the eddies transport momentum southward and upward across the unstable u_E part of the jet and northward across the stable u_M part. The latter flux is consistent with the northward heat transport and the southward wave progagation — as the eddy geopotential fluxes in Fig. 17b and d confirm. The winter westerly, on the other hand, has a poleward-traversing flux and the same QG_γ character as the DRY midrange jets. The QG_γ westerly does not change into multiple QG_β jets as Ω^* increases because it remains wide and retains a β variation that encourages an asymmetric, equatorward wave dispersion. The eddies thus support all westerlies and reduce all easterlies, as in Fig. 17c.

Although the $\overline{v'M'}$ fluxes generally change little in form as θ_p and Ω^* vary, the following variations in Fig. 16 are notable: (1) in the hybrid OBLIQUE(Ω^*, 10°) states, the additional summer westerly has a QG_γ flux; (2) in the OBLIQUE(Ω^*, 25°) flows with $\Omega^* \geq 1$, the additional equatorward flux in the summer midlatitudes helps converge momentum onto the westerly tradewind; (3) in the OBLIQUE(½, 25°) westerly, the flux is weak because the instability is relatively shallow (as is the Ferrel cell); (4) in the OBLIQUE(Ω^*, 90°) flows with $\Omega^* \geq 1$, the easterly's low-level flux dominates; and (5) in the exceptional OBLIQUE(½, 90°) case, the fluxes are uniquely equatorward in both hemispheres, with the deep summer flux and the confined winter flux reducing the easterly flow and reflecting the

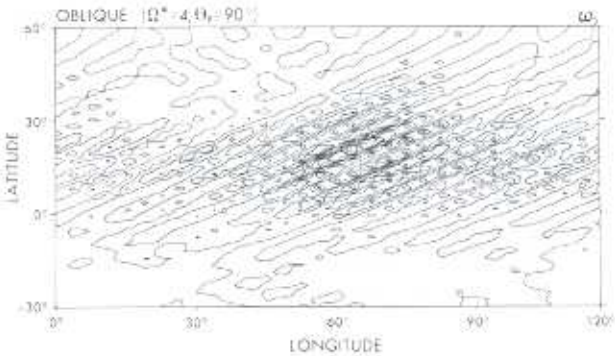

Fig. 18. Latitude-longitude distribution of the instantaneous vertical pressure velocity at 515 mb in the OBLIQUE model with $\Omega^* = 4$ and $\theta_p = 90°$. This illustrates a special form of baroclinic instability in the easterly jet. Units: 10^2 mb s^{-1}

baroclinic instability and the wave propagation, respectively.

A synoptic anomaly. The exceptional form of disturbance shown in Fig. 18 occurs in the OBLIQUE(4,90°) summer hemisphere, between latitudes 0° and 30°N, during a high-resolution extension of the basic solution. The disturbance peaks in the Hadley cell's upflow, lasts for 30 days, and takes the form of diagonal bands of vertical motion. The bands have a longitudinal wavenumber of 30 and are well resolved by the R42 model, but are excluded by the R15 model. The disturbance has an environment whose surface temperatures go from 150 K at the equator, to 270 K at 30°N — to produce an intense baroclinicity, but little moisture — and whose easterly jet goes from -50 ms^{-1} at the equator, to -10 ms^{-1} at 30°N — to give strong vertical and lateral shears. We believe the disturbance is caused by a baroclinic instability that is differentially advected by the easterly jet. The Rossby radius and the jet width determine the scale and extent of the bands.

The budgets and balances (Table 2, Figs. 19, 20). The global mean temperatures of the OBLIQUE states, like those of the previous sets, all approach Earth's effective temperature, despite the large interhemispheric heating variations (Table 2). (The lower values are due to reductions in the solar constant at higher θ_P.) The global mixing ratio drops at higher tilts because the moisture is confined to regions north of $\theta = 30°$S, 0° and 30°N when $\theta_P = 10°$, 25° and 90°, respectively. The eddy kinetic energy and the eddy fluxes remain nearly constant as Ω^* increases (for a given θ_P) because the eddies remain strong as their sources

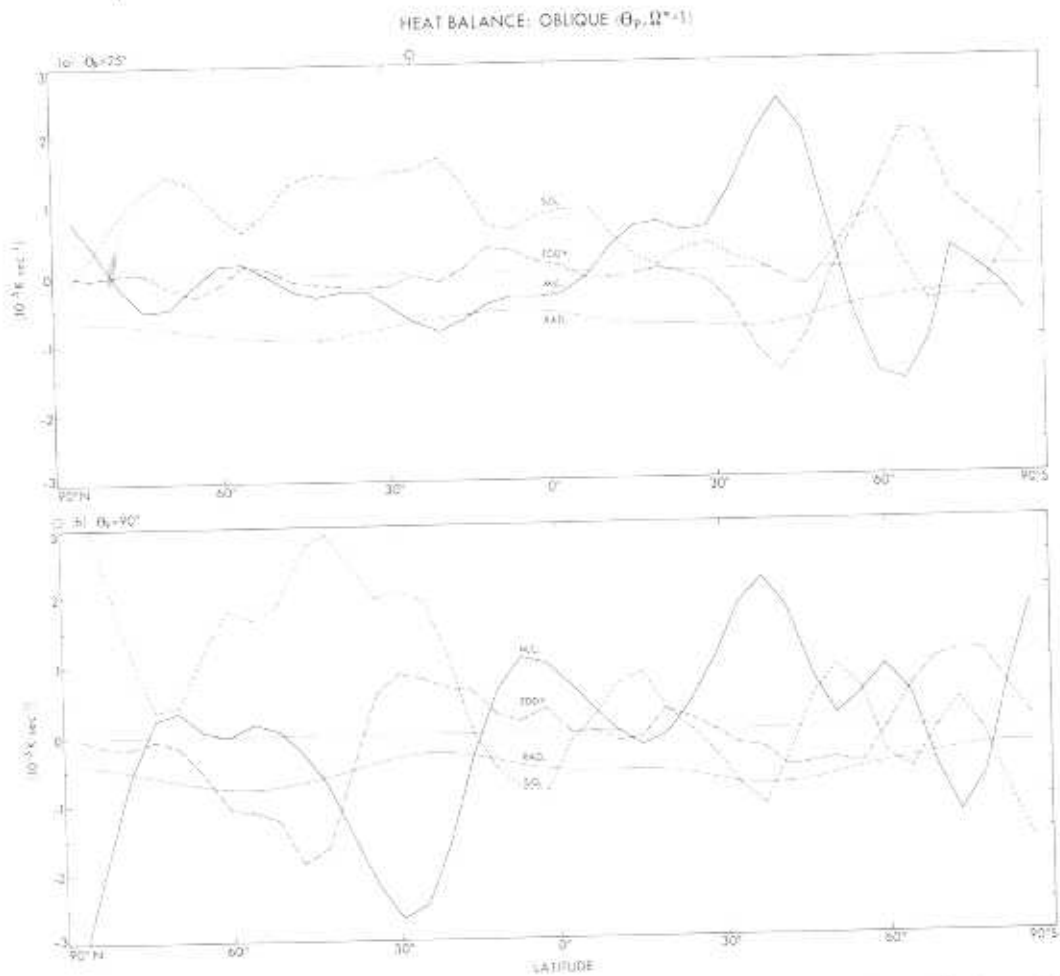

Fig. 19. Latitudinal distribution of the contributions to the mean rate of temperature change by the meridional circulation (*M.C.*), the eddies (*EDDY*), the radiation (*RAD*), and the subgrid processes (*S.G.*) in the OBLIQUE model with $\Omega^* = 1$, $\theta_P = 25°$ and 90°. Units 10^{-5} K s^{-1}

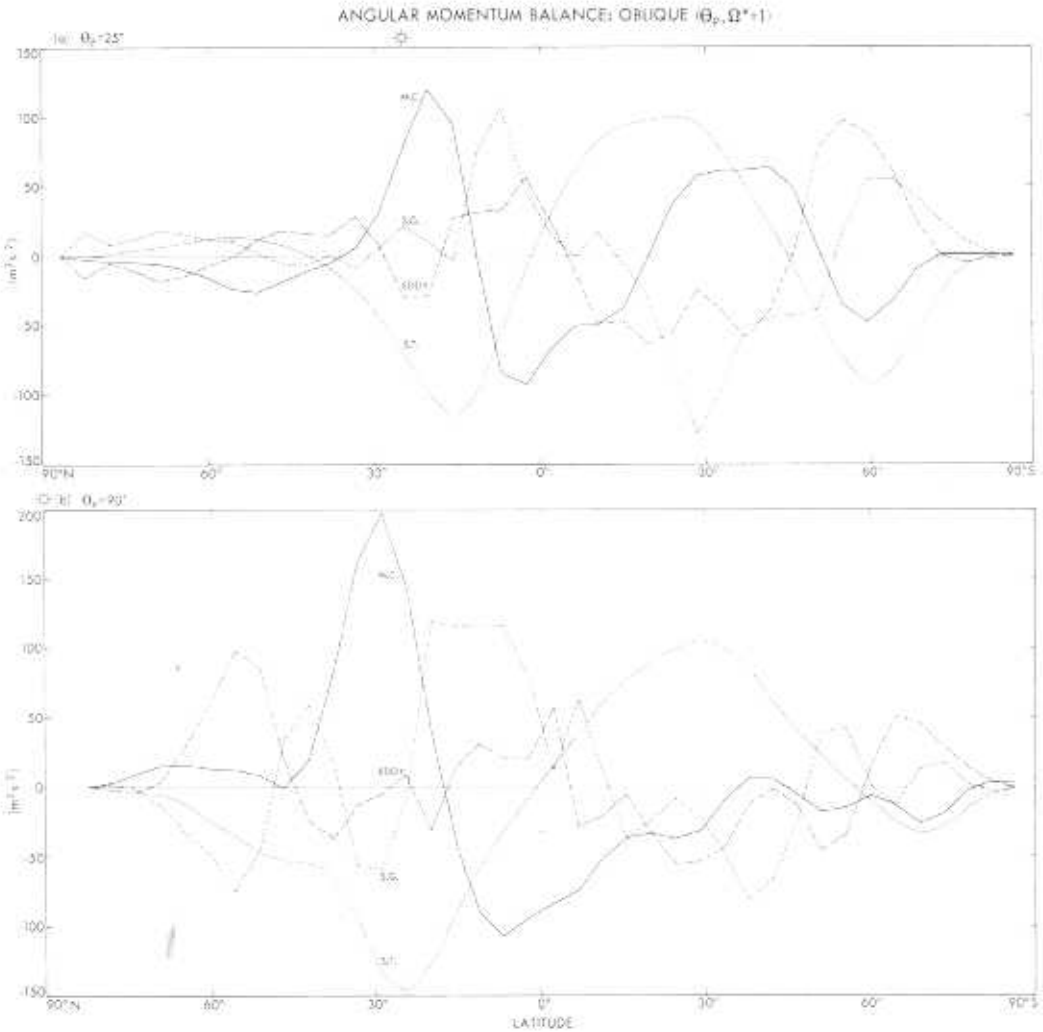

Fig. 20. Latitudinal distribution of the contributions to the mean rate of angular-momentum change by the meridional circulation *(M.C.)*, the eddies *(EDDY)*, the surface torque *(S.T.)*, and the subgrid diffusion *(S.G.)* in the OBLIQUE model with $\Omega^* = 1$, $\theta_p = 25°$ and 90°. Units: $m^2\ s^{-2}$

move equatorward. The mean kinetic energy, however, has a substantial range, from 45 to 2990 J kg^{-1}, with the exceptional OBLIQUE (½,90°) state having the largest — perhaps the maximum possible — value.

The solstitial heat and momentum balances mainly change their meridional scale, not their form, as the parameters vary and may be represented by the typical OBLIQUE(1,25°) state and the extreme OBLIQUE(1,90°) state. In the typical case, the moist summer hemisphere is heated by the convection at all latitudes, and cooled by the radiation and the Hadley cell (Fig. 19a). The convection follows the solar input, peaking at 70°N and driving a secondary cell whose subsidence creates the polar hot spot. The dry winter hemisphere is heated by the Hadley cell's subsidence as far as 50°S, with the eddies then heating the higher latitudes and inducing a compensating Ferrel cell. A similar heat balance occurs in the high-tilt case in Fig. 19b, except that now the eddies also cool the summer midlatitudes and a direct cell cools the summer pole. The radiative cooling fields in Fig. 6b and d show the thermal forcing to be relatively uniform and to have rates comparable with the MOIST midrange, despite the existence of a dry, unlit winter hemisphere.

In the OBLIQUE(1,25°) momentum balance in Fig. 20a, almost equal amounts of the momentum produced by the easterly tradewinds (in $\theta = 0°$–45°S) are transported northward and southward; north across the equator by the Hadley cell to balance the sink in the westerly tradewinds, and south into midlatitudes by the eddies to balance — through the Ferrel cell — the sink in the westerly jet. In the OBLIQUE(1,90°) balance

in Fig. 20b, the easterly jet supplements the easterly tradewinds in producing a strong momentum source over a wide region ($\theta = 0°$-$60°$S) in the winter hemisphere. Most of this supply is transported northward across the equator by the Hadley cell to balance the sink produced by the hemisphere-wide westerly tradewinds. The eddies extend the transport into high latitudes in both hemispheres.

4 DIURNAL(LOW Ω^*) circulations

Circulations in the low singular range ($0 \leqslant \Omega^* \leqslant 1/16$) are essentially natural-Hadley elements whose mean zonal flows restructure their balance during the asymptotic transition, and whose eddies are enhanced during the diurnal transition. To understand such flows, we need a theory describing the propagation of large planetary waves in symmetric-Hadley states at low Ω^*. Little is known about this dynamical regime, so our presentation is mainly descriptive. The singular-range circulations are important, however, and are relevant to slowly rotating planets such as Venus and Titan (see Hou 1984, Rossow 1983, 1985).

To define the diurnal and asymptotic transitions, we evaluate the moist GCM, with and without the diurnal heating, for $\Omega^* = 1/16$, $1/32$ and $1/64$, and refer to the two groups of solutions as the diurnal DL(Ω^*) and nondiurnal NDL(Ω^*) circulations. The diurnal, asymptotic and Halley transitions follow one another closely as Ω^* decreases over the singular range: the diurnal effects become vital as Ω^* approaches $1/16$, the asymptotic transition occurs between $\Omega^* = 1/16$ and $1/32$, and the Halley mode emerges between $\Omega^* = 1/32$ and $1/64$. Diurnally modified NH elements — in which diurnality boosts the planetary waves and the eddy fluxes — occur in the outer singular range ($\Omega^* > 1/48$), while diurnally dominated Halley flows — in which the atmosphere moves mainly from the subsolar to the antisolar region — occur in the inner singular range ($\Omega^* < 1/48$). Solutions at $\Omega^* = 1/48$ and $1/128$ help define the Halley transition and state, but they differ so little from the solution at $\Omega^* = 1/64$ that only their integrals are documented (in Table 3).

Diurnal variations are included in the GCM by prescribing a time-dependent zenith angle as a function of the length of the solar day. The relations $(\tau_A, \tau_O, \tau_S) = 2\Pi/(\Omega, \Omega_O, \Omega_S)$ define the sidereal day, the sidereal year and the solar day in terms of the planet's axial and orbital angular velocities, and the sun's angular motion across the planet's face, where $\Omega_S = \Omega - \Omega_O$. For Earth these periods are disparate and equal 1.0, 366.26 and 1.003 days, while for Venus they are all comparable and equal -245, 225 and -120 days; where a 'day' denotes the terrestrial sidereal period (23.934 hours), and where the negative sign symbolizes retrograde motion. Integrations with the GCM in a Venus-like retrograde configuration produce solutions that resemble the standard DL(Ω^*) states, so are not presented. Most calculations use a minimally adequate R15 horizontal resolution, together with 360° and 120° hemispheric domains for the diurnal and nondiurnal systems, respectively (Table I-1). The NDL($1/16$) case is equivalent to the MOIST($1/16$) case, and it alone has a higher (R30) resolution.

Diurnality can act either directly through the radiation or indirectly through the convection and the PBL mixing. In the standard GCM the diurnal forcing is mostly convective and mostly confined to the lower atmosphere, even though the response is felt aloft. To examine how a radiative diurnality behaves, we create a special HIGH-CLOUD model that incorporates a single opaque (100% cover) cloud near the 300-mb height to increase heating in the upper atmosphere; all other clouds are removed, but a small amount of ozone is kept in the stratosphere. The new cloud has an albedo of 0.6 and an absorptivity of 0.2, so only 20% of the solar radiation reaches the lower atmosphere. The solar constant is then doubled to try to maintain a normal temperature range. The HIGH-CLOUD model, evaluated at $\Omega^* = 1/64$ for the diurnal (HCDL) and nondiurnal (HCNDL) configurations, remains relatively cool and, hence, illustrates how a nearly dry atmosphere responds to diurnal forcing.

4.1 *The basic fields (Figs. 21–25)*

The NDL system. The natural-Hadley element of the MOIST low range, with its polar jet and broad Hadley cell, persists in the NDL singular-range circulations (Figs. 21–24, cols. 1). But major changes occur when the cell reaches the pole and sets up the asymptotic transition between $\Omega^* = 1/16$ and $1/32$: the jet loses two-thirds of its momentum and halts the poleward migration of its axis at $\theta = 75°$, while the surface baroclinicity drops sharply from 40 K to 10 K and a new jet arises in the stratosphere. Although all NDL jets have momentum-wind features — vertical contours and shears that increase with latitude — their amplitudes drop from 80% to 50% of $u_M(75°)$ during

Table 3. DIURNAL circulations: energy, heat and momentum integrals

Case				Energy					Heat					Momentum				
Ω^a	Q_E	Δ	τ_I	K_Z	K_E	$P{:}K_Z$	$P{:}K_E$	$K_Z{:}K_E$	T^a	r^a	RAD	v^*T^{*c}	$-\omega^*T^*$	Max^b torque	v^*M^{*c}	$-\omega^*M^*$	Max^b $\lvert u\rvert^0$	Max $\lvert v\rvert$
1/16	NDL	D	909	286	21	162	36	51	253.1	2.0	− 921	309	132	−8.0	−179	− 70	81	7.6
1/32	NDL	A	720	70	41	148	38	23	252.9	2.1	− 926	33	131	−4.7	−236	− 56	29	8.5
1/48	NDL	A	480	34	33	122	56	8	252.8	2.0	− 926	38	109	−2.5	−159	− 33	20	8.9
1/64	NDL	A	480	23	30	128	57	6	252.5	2.1	− 930	28	113	−1.5	−137	− 16	13	9.1
1/128	NDL	A	400	13	26	103	41	2	252.3	2.1	− 933	22	100	−0.7	− 35	− 67	6	9.1
1/16	DL	C	595	576	137	387	52	192	257.6	2.6	−1141	−219	366	5.3	−899	−499	57	5.5
1/32	DL	C	830	261	170	227	219	80	258.3	2.1	−1189	−552	1263	2.3	−564	−224	37	4.9
1/48	DL	C	470	73	140	181	300	9	257.9	1.6	−1218	−825	793	1.1	−397	−254	20	5.9
1/64	DL	C	520	40	134	151	337	7	257.8	1.6	−1229	−838	838	0.7	−233	−138	14	6.5
1/128	DL	C	390	11	106	122	319	0	258.2	1.5	−1239	−866	803	1.1	− 89	−214	7	7.3
1/64	HCNDL	A	560	24	13	47	−2	3	228.2	0.4	− 152	− 7	6	−2.9	− 79	− 2	14	8.0
1/64	HCDL	C	360	29	82	84	116	−1	232.4	0.3	− 350	−261	294	0.8	−151	−189	14	3.2
Units			Days	$J\ kg^{-1}$		$10^{-6}\ W\ kg^{-1}$			K	cm water	$10^{-8}\ K s^{-1}$	$10^1\ J\ m\ kg^{-1}\ s^{-1}$	$10^{-2}\ W\ m^{-2}$	$m^2\ s^{-2}$	$10^5\ kg^2\ m^{-2}\ s^{-2}$	10^2	$m\ s^{-1}$	

[a] Instantaneous values
[b] Local values
[c] Symbolic notation for eddy transports
[0] In troposphere only

Q_E denotes heat form: NDL ≡ nondiurnal, DL ≡ diurnal
HC denotes HIGH CLOUD supplementary case with solar constant doubled
Δ denotes domain and resolution: see Table 1 of Part I
τ_I denotes integration period
RAD denotes radiative heating rate

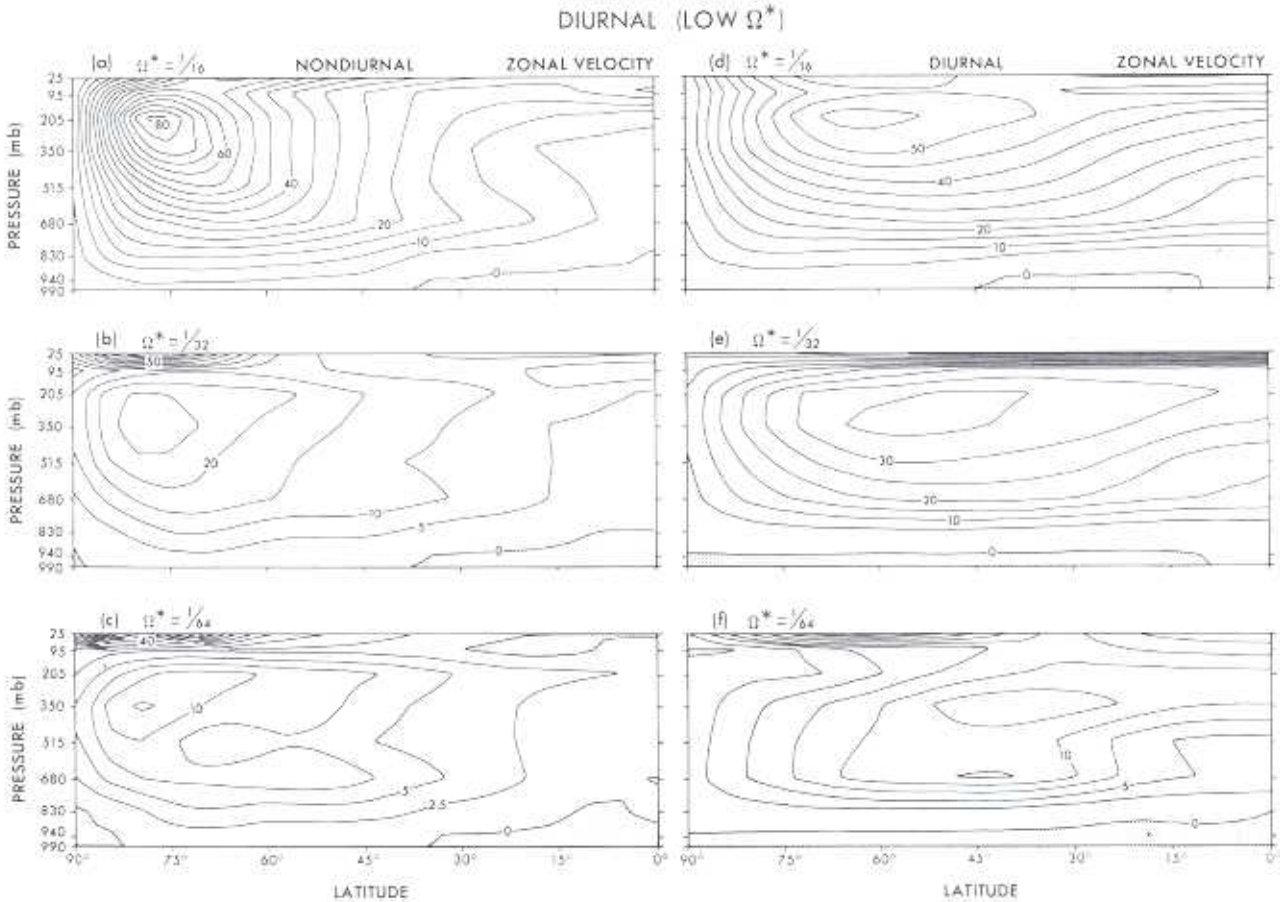

Fig. 21. Meridional distribution of the mean zonal wind in the DIURNAL model with nondiurnal *(left column)* and diurnal *(right column)* heating for $\Omega^* = 1/16$–$1/64$. Units: ms^{-1}

the transition, presumably because the eddies and the detrainment from the upper troposphere become more effective. After the transition, the cell and the temperature field remain almost invariant at the MOIST(0) values, while the jet and the eddies continue to weaken with Ω^*. The NDL eddies in Fig. 24 retain the main NH features throughout: a peak activity and a latitudinal invariance in the upper troposphere.

The DL system. Adding diurnal heating to the singular-range NH flows boosts the amplitude of the eddies and, thereby, strengthens, broadens and moves the jets to lower latitudes (Figs. 21–24, cols. 2). The DL(1/16) and DL(1/32) circulations are equivalent to diurnally modified NH elements whose planetary waves have been strengthened by the localization of the moist convective forcing. The DL(1/64) circulation, on the other hand, is a diurnally dominated Halley element with a prevailing subsolar to antisolar flow. Although the Halley zonal-mean fields still have the modified NH form, they are insignificant, given that the jet and cell lack longitudinal continuity when $K_E \gg K_Z$ (Table 3). The asymptotic transition is still discernible in the sharp baroclinicity drop, but is otherwise submerged by the strong diurnal transition.

The diurnally boosted planetary waves completely reverse a jet's tendency to migrate poleward as Ω^* decreases, to the extent that it actually reaches the equator at the Halley transition (when $\Omega^* = 1/45$), Fig. 21f. Although the DL jets compare closely with their NDL counterparts in amplitude, they actually have 3–4 times more kinetic energy — because they are broader, super-rotating, and midlatitudinal (Table 3). Clearly, diurnality both creates and redistributes westerly momentum. The PBL easterlies become global when $\Omega^* = 1/64$, so the Halley flows either retard the planet's rotation or have vanishing mean surface winds. Although the diurnality acts through the planetary wave fluxes to weaken the meridional circulation by about 30%, the Hadley cell actually develops a

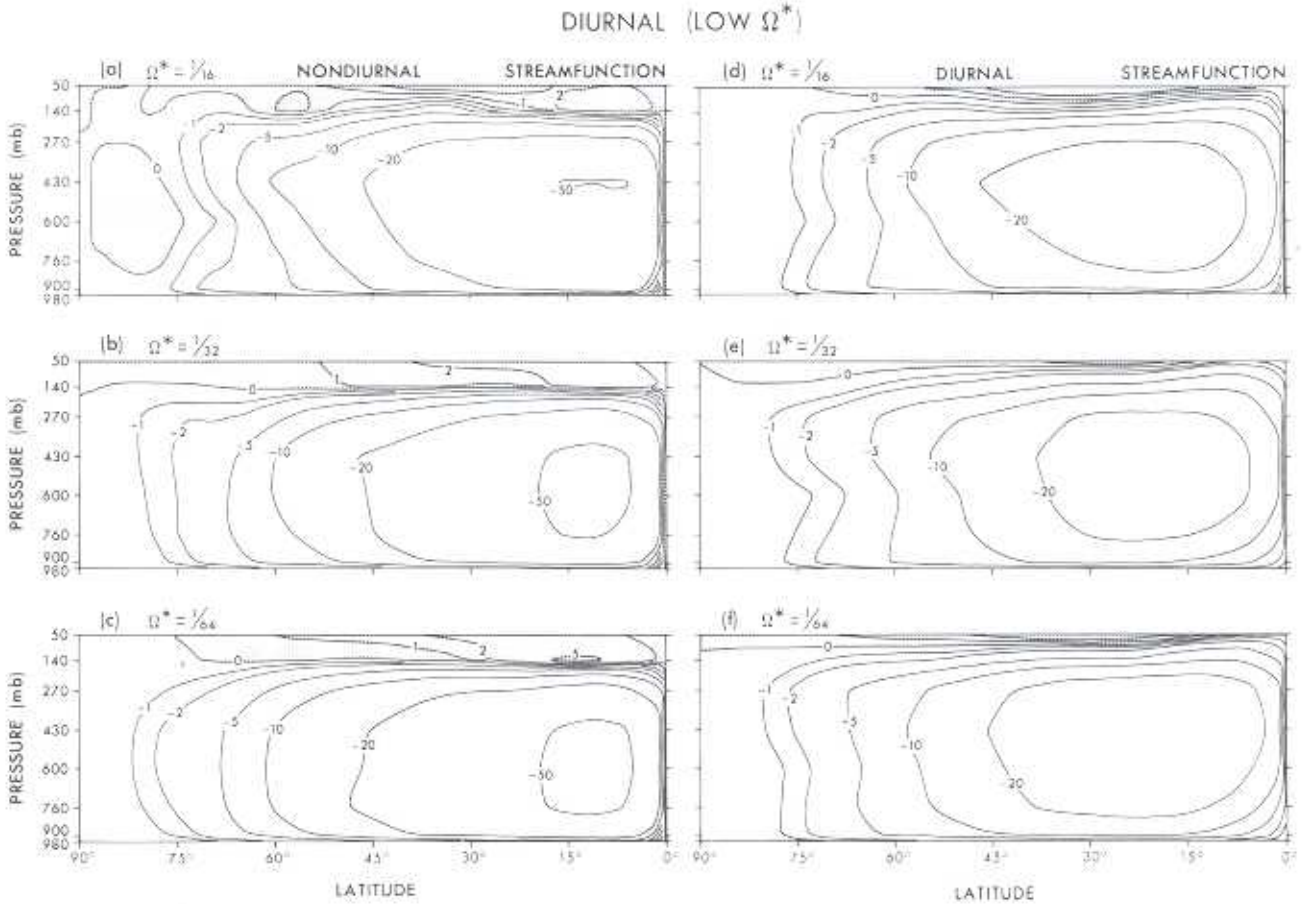

Fig. 22. Meridional distribution of the mean stream function in the DIURNAL model with nondiurnal *(left column)* and diurnal *(right column)* heating for $\Omega^* = 1/16$–$1/64$. Units: 10^{13} gs^{-1}

broader upflow that cools a wider region (see Fig. 31b) and reduces the mean baroclinicity by 5–10 K (Fig. 23). The temperature field, however, still contains intense latitudinal and longitudinal gradients in the subsolar hotspot.

The eddies produced by the diurnality in the singular range are actually stronger than the eddies produced by the baroclinicity in the mid-range, but they have the broader (k^{-2}) energy spectrum typical of low-range flows (Fig. I-15). The DL eddy kinetic energies in Fig. 24 are relatively independent of θ and Ω^* and are produced, presumably, by the same types of wave as occur in the NDL circulations. Our analysis does not identify the waves, but they appear to behave just like Rossby waves in Earth's tropics (Hayashi 1974), transporting heat and momentum equatorward. Other planetary waves, such as the Kelvin and Yanai modes, also become hemispheric in scale at low Ω^* but, given the absence of an upward momentum flux, would appear to be inactive. Localized (Pacific Ocean) hotspots are known generators of Rossby waves in the terrestrial case (Webster 1983), and the DL hotspots — although mobile and hemispheric — probably produce low-Ω^* planetary waves in a similar way. Planetary waves with the lowest wavenumbers tend to dominate the flow fields because only they are barotropically stable for triad resonances in the singular range (Baines 1976, Rossow and Williams 1979).

The HIGH-CLOUD system. Adding an upper-level radiative heating to the GCM through the HIGH-CLOUD formulation produces a unique circulation — two vertically stacked jets and three vertically stacked cells — but only in the nondiurnal configuration (Fig. 25, col. 1). The lower component of the HCNDL circulation has the same features and dynamics as a dry NH element: a polar jet that peaks at $\theta = 75°$, a cell that extends to the jet axis, and weak eddies generated by barotropic cascades in the jet core. Above it, the upper component has a midlatitudinal jet that peaks at

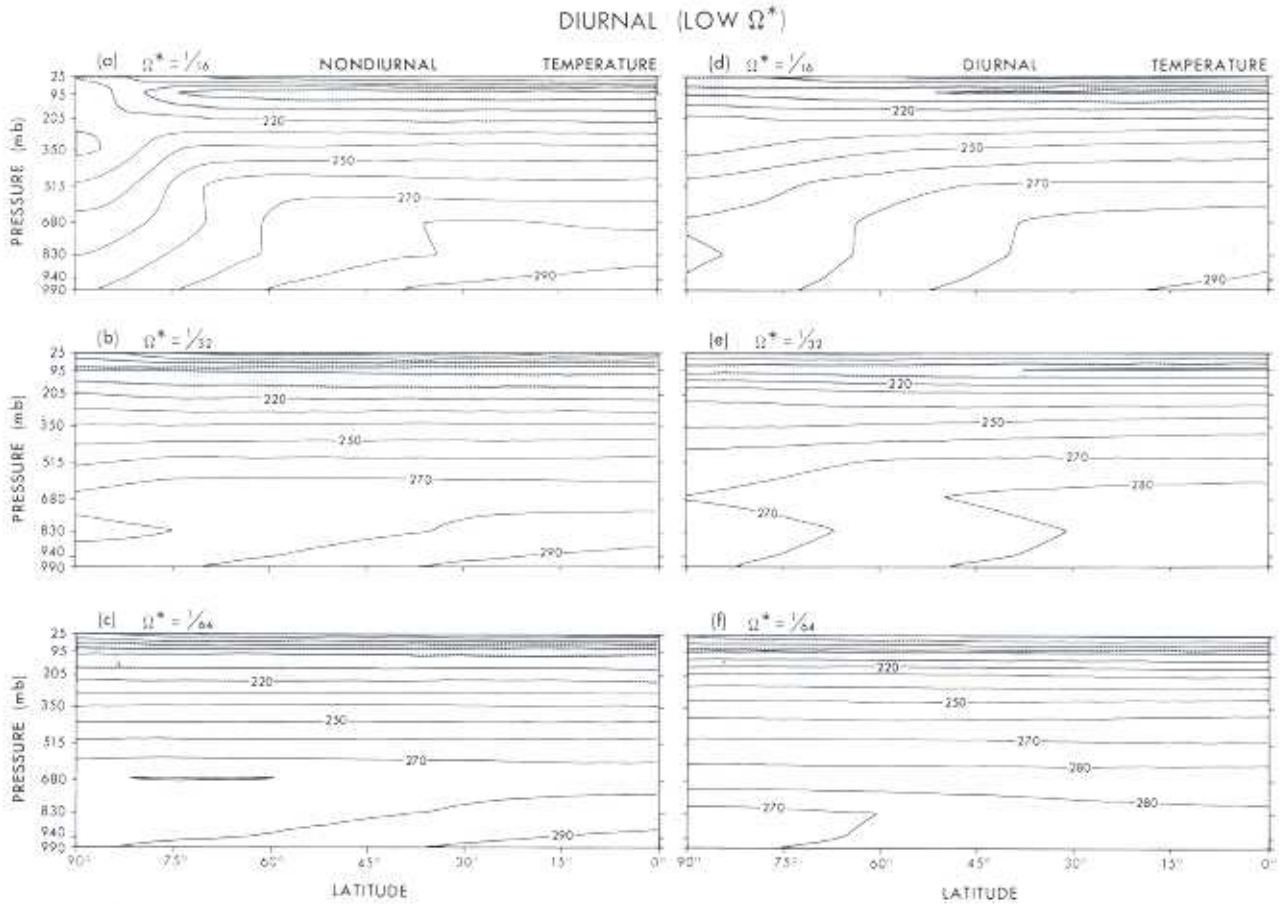

Fig. 23. Meridional distribution of the mean temperature in the DIURNAL model with nondiurnal *(left column)* and diurnal *(right column)* heating for $\Omega^* = 1/16$–$1/64$. Units: K

$\theta = 50°$, and a cell that extends beyond the core (to $\theta = 75°$) and appears to be purely thermally driven by the radiative gradient (Fig. 6c). This upper jet cannot develop an SH_1 momentum wind because it lacks direct contact with the surface. Indeed, the SH_1 theory can say little about vertically complex flows whose depth is controlled by the radiation field, rather than by the scale height.

Subjecting the HIGH-CLOUD system to diurnal heating removes the above idiosyncracies and restores the standard DL(1/64) form of circulation (Fig. 25, col. 2). The simple (single-cell, single-jet) form is re-established because the momentum fluxes associated with the strong planetary waves take over from the diabatic driving in shaping the mean circulation. These planetary waves have the same form and same upper-level location regardless of the height at which the diurnal forcing is applied. The HCDL eddies in Fig. 25h, however, have only half as much kinetic energy as the DL(1/64) eddies because the system is quite dry, even though localized 300-K temperatures and moist convection occur.

4.2 The eddy fluxes (Figs. 26–30)

Because the eddy fluxes maintain their form throughout the low range, they can be used to classify the eddies in the singular range, even though zonal averaging becomes less meaningful when $\Omega^* \to 0$. Only the diurnal eddy fluxes are presented here; the nondiurnal fluxes are weak and represented elsewhere by the MOIST(1/16) solution in Figs. 1-6i-9i.

The diurnality produces strong equatorward heat fluxes both directly in the thermal wave at low levels, and indirectly in the planetary waves at upper levels (Fig. 26). The diurnality also extends the moist convection into higher latitudes in the subsolar hotspot and, thereby, expands the mean upward eddy heat flux (or baroclinic conversion) from $\theta = 10°$ to $\theta = 30°$ (Fig. 27). This

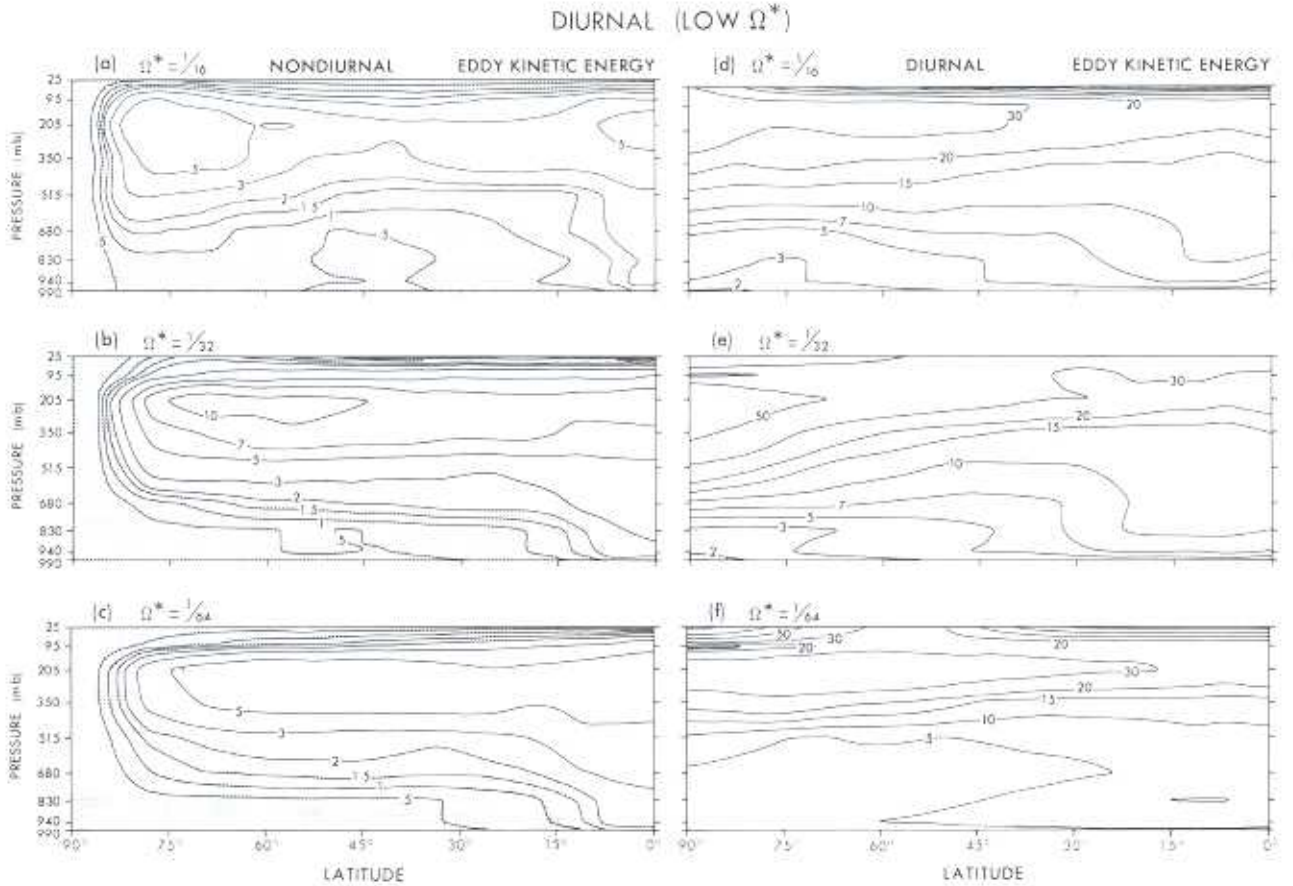

Fig. 24. Meridional distribution of the eddy kinetic energy in the DIURNAL model with nondiurnal *(left column)* and diurnal *(right column)* heating for $\Omega^* = 1/16$–$1/64$. Units: 10^4 J kg^{-1}

heat flux is vertically bimodal because the hotspot is limited to low levels. In Figs. 26c and 27c, the heat fluxes in the HCDL cloud are uniquely correlated — being poleward and upward — and imply that a baroclinic wave exists in the upper atmosphere.

The diurnally boosted convection also produces a better-organized, more-extensive vertical momentum flux than do the nondiurnal eddies (Fig. 28). This downward flux gives a measure of the planetary wave forcing. Once generated, the waves transfer momentum equatorward near the tropopause in both systems, but 5 times more strongly in the diurnal case (Fig. 29). The similarity between the $\overline{v'M'}$ fields of the standard and HIGH-CLOUD systems again shows that the height at which the diurnal forcing is applied influences only the wave amplitude, not the wave form. The forced thermal wave produces no momentum flux directly at low levels. In the unique HCNDL case, the momentum flux has two maxima, each associated with the barotropic cascade of a stacked jet (Fig. 29c).

The influence of the diurnality on the momentum transfer can also be seen in the midlevel geopotential field of the DL(1/32) case in Fig. 30b. These instantaneous Φ_5 contours act as a stream function in higher latitudes ($\theta > 45°$), showing that the atmosphere flows gradually toward the subsolar region but then moves poleward to avoid the hotspot. Such flows transport momentum poleward, as in the lesser $\overline{v'M'}$ component in Fig. 29e. The Φ_2 geopotential field has even steeper gradients, suggesting that the planetary waves are close to breaking in the upper atmosphere. The flow in low latitudes, as illustrated by the midlevel u_5 field in Fig. 30c, also forms a continuous westerly jet — except at the equator, where there is a weak easterly flow into the hotspot. The subsolar hotspot, as defined by the 280-K contour of the lowest-level temperature T_9 in Fig. 30a, extends over 60° of latitude and 180° of longitude

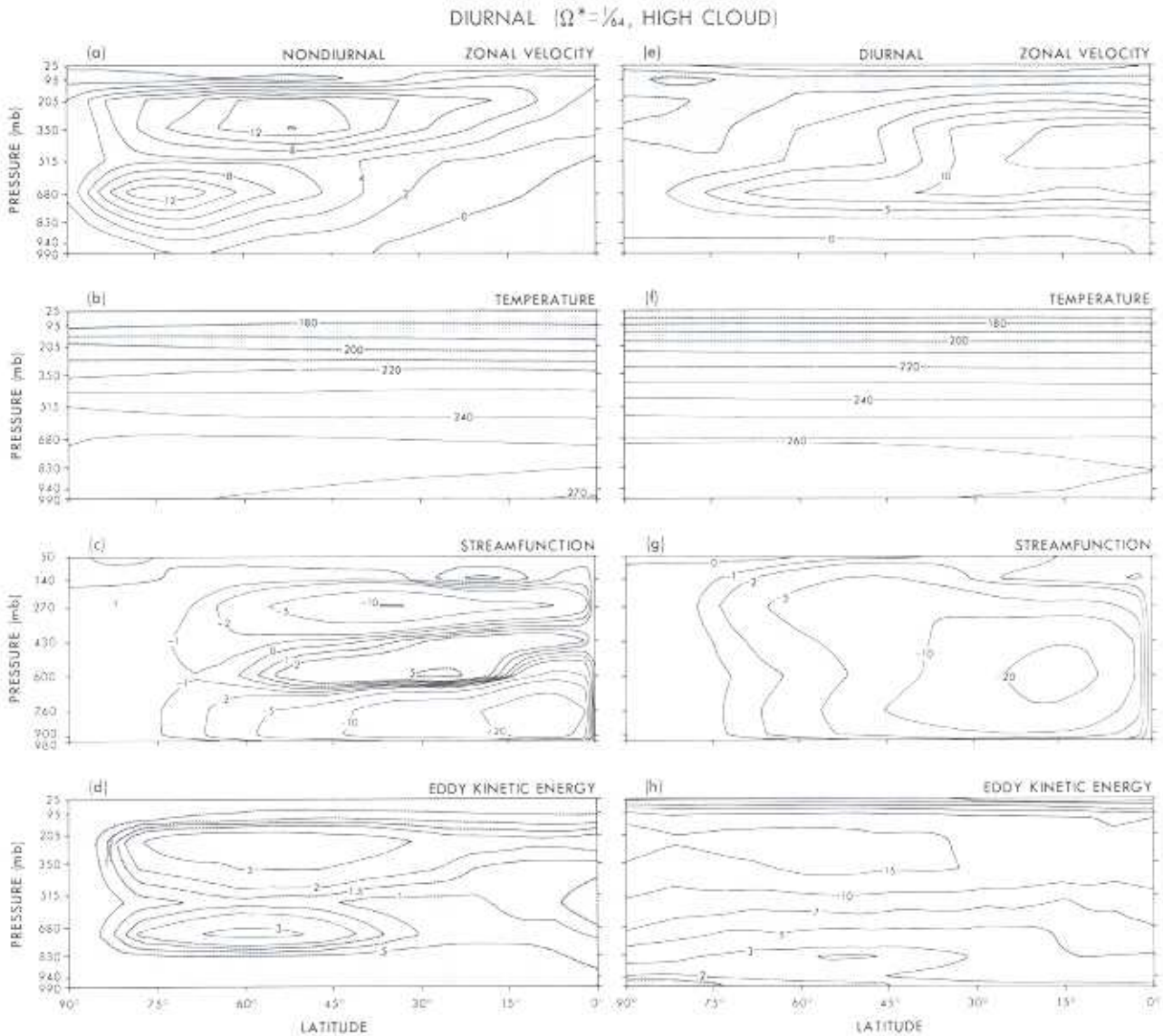

Fig. 25. Meridional distribution of the mean zonal wind, temperature, stream function, and eddy kinetic energy in the HIGH-CLOUD model with nondiurnal *(left column)* and diurnal *(right column)* heating for $\Omega^* = 1/64$. Units: m s^{-1}, K, 10^{13} g s^{-1}, 10^1 J kg^{-1}

and reaches a peak of 310 K, while allowing a relatively isothermal (275 ± 5 K) unlit hemisphere. The hotspot is relatively shallow: the T_7 contours are open and trail to the east as the spot moves westward.

4.3 The budgets and balances (Table 3, Fig. 31)

The diurnally heated atmospheres are the only systems whose global temperatures deviate significantly (by +5 K) from Earth's effective temperature, but the reason remains obscure. The diurnality also produces a substantial increase in all the energy, conversion and flux integrals listed in Table 3; only the cell strength and the surface drag are reduced. The radiative cooling rates are increased by 30% because the moisture, although reduced globally, lies in the hottest regions.

The stacked cells give the nondiurnal HCNDL system a complicated heat balance by producing compensating fluxes: the lowest cell transports heat like a Hadley cell — equatorward below and poleward aloft — while the central and upper cells transport heat only one way — equatorward and poleward, respectively. Together, the three cells cool the equator and midlatitudes and heat the pole and subtropics (Fig. 31a). The diurnal

HCDL system, on the other hand, has a simpler balance because its single cell has a broad upflow like a dry Hadley cell and cools a wide region ($\theta = 0°$-$25°$) in response to the heating by the hot-spot convection and the diurnal eddy flux (Fig. 31b).

5 Planetary circulations

The planets have diverse configurations and can test circulation theory in parameter regions that are inaccessible to Earth. Although observations are still limited, the remote planets are in principle no more remote than the ancient terrestrial climates and could be equally useful. Many of these atmospheres should have the same circulation forms as the GCM solutions because the rotation places such a dominant constraint on the large-scale motions, limiting their variety to a few basic types (Williams and Holloway 1982; Williams 1985). In fact the meteorology of the solar system could be relatively simple, unified, and GFD-based. Consequently, in this section, we try to classify the various planetary circulations and the theories they relate to.

5.1 Circulation factors and model range

Circulation form depends not only on the rotation and the obliquity but also on the atmospheric structure, depth, heat supply, and phase changes. Of the latter factors, the structure has the most fundamental influence and lies between the two limits defined by: (1) a bounded (semi-infinite) atmosphere having a solid or fluid sublayer like the terrestrial planets; and (2) an unbounded or thermally confined layer having an underlying abyss like the Jovian planets and Earth's ocean. Compared to the bounded states described by the GCM, an unbounded atmosphere should have a greater thermal inertia, a weaker dissipation and a more internal form of baroclinic instability, and should cascade further toward a zonal, barotropic end-state. It must, however, experience some drag and frictional interaction with the abyss for the influence of $\mathbf{\Omega}$ to be communicated; free-slip states are not realistic.

The thermal factors mainly influence the diurnal and seasonal variability. Whether an atmosphere is heated from above or below is dynamically immaterial, because either source can produce the baroclinicity to drive the large-scale flow and the convection to stabilize the system. The thermal inertia becomes important when a deep atmosphere has a radiative relaxation time $\tau_R(z)$ that exceeds the diurnal or seasonal periods at some depth. In general, the abyssal source and the thermal inertia tend to reduce the diurnal and seasonal variability. But in multiphase atmospheres, a condensational heating can add a strong dynamical variability in all ranges (cf. MOIST and DRY states), while sublimation can add a strong thermodynamical variability.

The structural and thermal factors are not varied in our GCM calculations, so their effect on circulations can only be deduced from simpler models. For example, quasi-geostrophic models show that bounded and unbounded atmospheres have essentially the same form of zonal motion in midlatitudes, even though their baroclinic instabilities differ (Williams 1979b). Thus, in midlatitudes, we expect future GCMs for unbounded atmospheres to develop $QG_{y,\beta}$ elements that have a stronger barotropic component, just as the SLIP models for bounded atmospheres do. In low latitudes, the various Hadley elements could survive in unbounded atmospheres — although they disappear in the SLIP states — if the weak drag needed to transmit $\mathbf{\Omega}$ is strong enough to support a momentum wind. Other simple models, such as the shallow water model, also apply to both structural forms and suggest that coherent vortices are the only phenomena unique to unbounded atmospheres (Williams 1985).

5.2 Planetary progression

We can classify the various planetary circulations to some extent by comparing them against GCM states with the same rotational configuration and implicitly allowing for structural and thermal differences, as follows.

Earth: the Ω^* midrange (moist). Earth, with its midrange rotation, medium tilt, and semi-moist surface, lies at the center of parameter space and offers data on the interactions between high and low latitudes, between the QG_y and QH elements. Near equinox, it has a blend of MOIST(1) and DRY(1) features and may be close to forming a double jet and transitional phenomena in midlatitudes. Near solstice, it tries to develop a baroclinically unstable easterly jet in the summer hemisphere — according to the OBLIQUE(1,10°) solution — but ocean heat prevents it from achieving the necessary negative baroclinicity (except in the stratosphere). Ocean heat can also prevent the de-

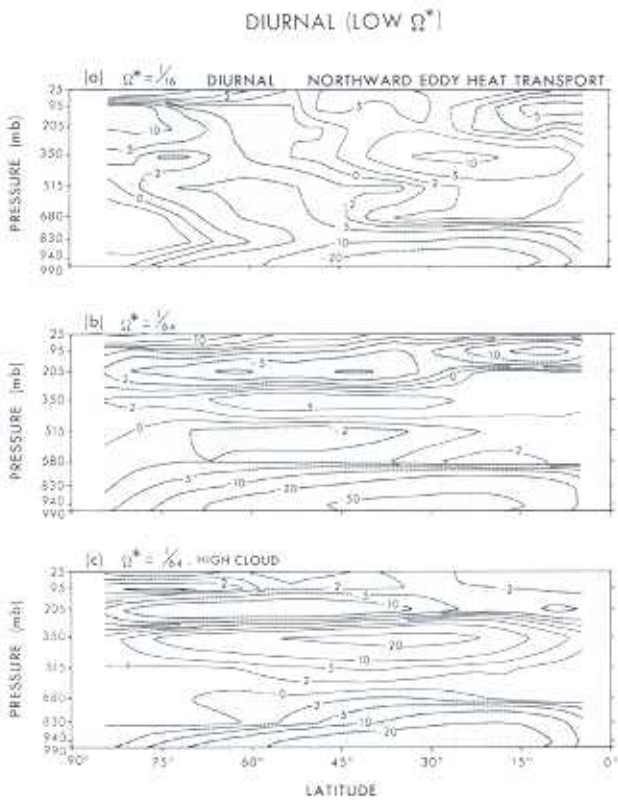

Fig. 26. Meridional distribution of the mean northward heat transport by the eddies in the diurnally heated DIURNAL model with $\Omega^* = 1/16$ and $1/64$ and the HIGH-CLOUD model with $\Omega^* = 1/64$. Units: 10^3 J m kg^{-1} s^{-1}

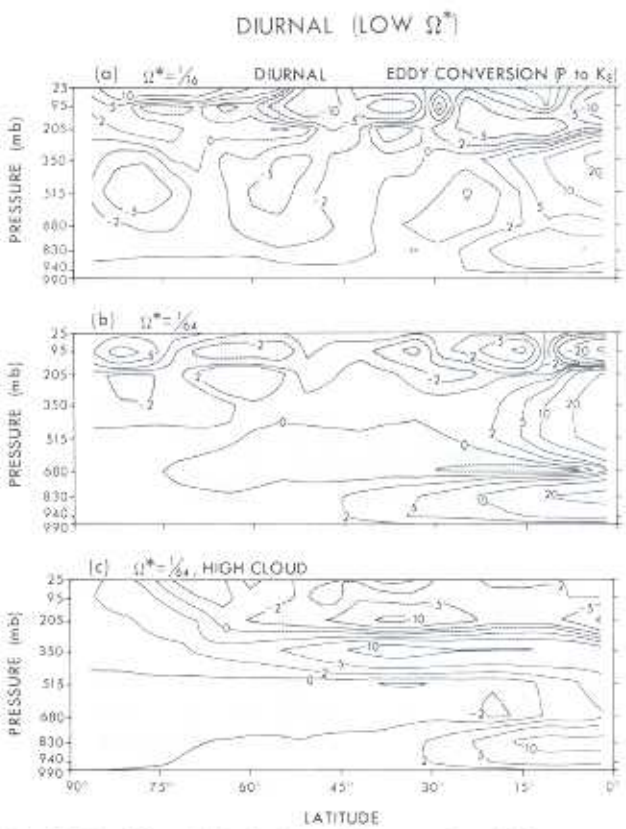

Fig. 27. Meridional distribution of the mean baroclinic energy conversion by the eddies, in the diurnally heated DIURNAL model with $\Omega^* = 1/16$ and $1/64$ and the HIGH-CLOUD model with $\Omega^* = 1/64$. Units: 10^{-4} W kg^{-1}

velopment of glaciation but fails to do so at higher rotation rates ($\Omega^* \geq 2$) — such as occurred during the Precambrian era (Hunt 1979a, b, Kutzbach 1985) — because the smaller atmospheric eddies (and the ocean currents they drive) transport too little heat poleward. Similar glacial extremes may occur in the future when $\Omega^* < 1/4$ and the eddies again become thermally inefficient.

Mars: the Ω^* midrange (dry). Mars lacks a sublayer constraint on seasonal variability and, therefore, provides a clearer example of solstitial flows, and a clearer test on the existence of the QGH element. Prediction models for Mars' dust-free (northern-summer) solstice produce a circulation resembling that of the OBLIQUE(3/4,15°) system: four zonal winds, two cells, a regular wave in the unstable winter westerly, and a peak T_s near $\theta = 60°$N (Leovy 1985, Fig. 2). The instability of the easterly jet, however, appears to be absent or undetected. In Mars' dust-storm (northern-winter) solstice, dust-loading increases the baroclinicity and the static stability, widens the Hadley cell, and pushes the peak T_s to the pole, to produce a circulation like that of the OBLIQUE(1,25°) system. Mars' obliquity oscillates between 15° and 35° over a period of 10^5 years and the changes in the seasonal variability appear to have been recorded in the layered deposits seen in the polar regions (Murray et al. 1981). Such layering could arise from the surface winds strengthening and shifting their peak from the winter to the summer hemisphere as θ_p increases, or from the particles becoming lighter when the poles are warmer.

Jupiter and Saturn: the Ω^* high range. Jupiter and Saturn have the same type of eddying, multi-jet zonal flow as the MOIST and HOT high-range circulations (Williams and Holloway 1982, Fig. 4, Williams 1985, Fig. 3) and, hence, relate to theories about the jet scales and the multi-element interactions. The weak drag and dissipation of these unbounded atmospheres allow a greater barotropy in the QG jets in midlatitudes, and a greater uncertainty about the Hadley flow in low latitudes. Saturn's thermal inertia and abyssal heat prevent that medium-tilt planet from developing a

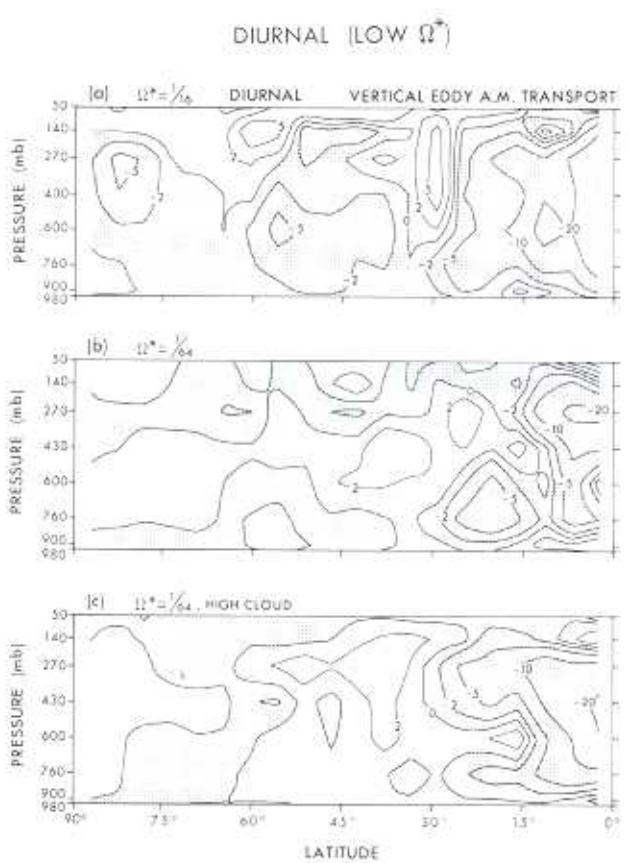

Fig. 28. Meridional distribution of the mean vertical angular-momentum transport by the eddies, in the diurnally heated DIURNAL model with $\Omega^* = 1/16$ and 1/64 and the HIGH-CLOUD model with $\Omega^* = 1/64$. Units: 10^2 kg s^{-2}

strong seasonal variability and, hence, from revealing the existence of Hadley dynamics through a QH to QGH element transition.

Uranus: an Ω^* midrange mystery. Before the Voyager encounter in 1986, it was hoped that Uranus' large (82°) obliquity would guarantee that the atmosphere show a large seasonal response and, thereby, expose the nature of Hadley modes in an unbounded system. But Uranus barely confessed its motion: only four isolated clouds were seen in the southern (summer) hemisphere, and these suggest the existence of a broad westerly jet that peaks at 55°S and an easterly flow that extends equatorward from 20°S — when measured relative to the magnetic frequency (Smith et al. 1986). These observations can be interpreted in at least three ways: (1) as a DRY(1) circulation, if the drag is strong and the seasonality is weak (because of the thermal inertia); (2) as a SLIP(1) circulation, if the drag and seasonality are both weak; and (3) as an OBLIQUE(1,25°) or OBLIQUE(1,90°) circulation, if the drag and seasonality are both strong, and if the flow is made entirely easterly by referring it to a faster-rotating frame. Changing the reference frame is not unreasonable, given that the magnetic rotation vector differs in direction from $\boldsymbol{\Omega}$ by 60°.

Titan: the Ω^* low range. Titan, with its slow (15.9-day) rotation, medium (27°) tilt, and substantial (1.6-bar) nitrogen atmosphere, provides an excellent system for testing axisymmetric circulation theory over the full range of seasonal variation. Titan's circulations should vary from the low-range SH element at equinox to the SSH element (with a pole-to-pole cell) at solstice. As yet, no winds have been measured nor any longitudinal variation seen, but large seasonal variations have been detected in the albedo that could be related to a cycle in the Hadley mode.

Venus: the Ω^* singular range. Venus' stratosphere has the same type of broad, super-rotating westerly current as the diurnally modified, singular-range GCM solutions — such as DL(1/32) — and, therefore, relates to various theories about the NH elements, particularly about how the vertical structure modifies their mean flows, wave propagation, and diurnal transitions. Although the diurnal component of the heating is thought to be confined to Venus' stratosphere by the large opacity and long τ_R of the troposphere (Rossow 1985), it could still generate planetary waves that are amplified as they propagate upward over many scale heights to produce a strong equatorward momentum flux and a broad jet in the upper atmosphere. The lower atmosphere could remain immune to the diurnality and contain a simple polar jet or multiple stacked jets. Venus' circulation has been difficult to understand because the planet lies in a parameter range where the zonal flow is sensitive to thermal details, and where the meridional flow — the essential Venus — is dominant and yet to be observed.

6 Conclusions

We have examined the influence of various hemispheric asymmetries on circulation form by varying the rotation rate for axisymmetric, oblique and diurnal GCMs. Varying Ω^* changes the Rossby and Froude numbers and alters the scale and mix of the jets, cells, and eddies. We can then isolate the invariant features of each system and identify their QG and Hadley modes. In particu-

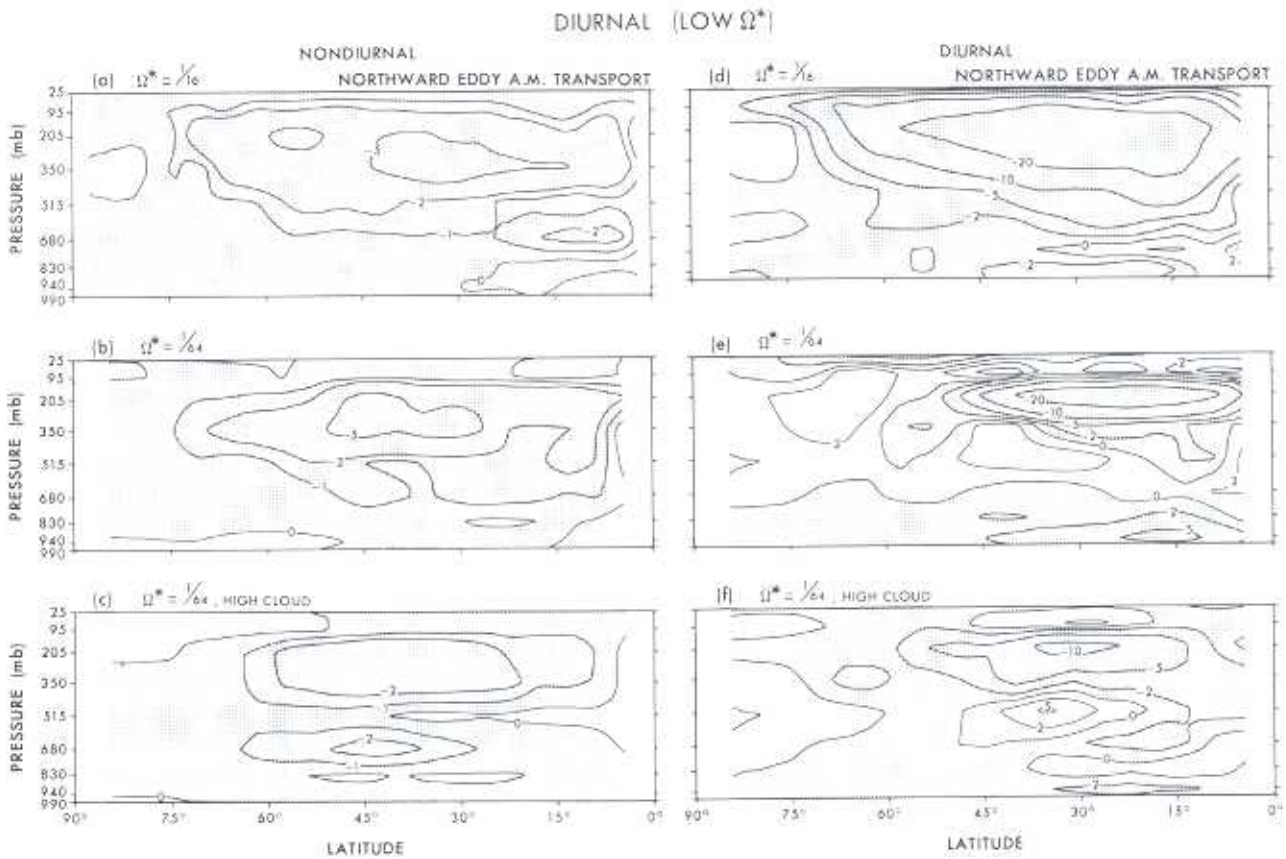

Fig. 29. Meridional distribution of the mean northward angular-momentum transport by the eddies, in the DIURNAL model with $\Omega^* = 1/16$ and $1/64$ and in the HIGH-CLOUD model with $\Omega^* = 1/64$, for nondiurnal and diurnal heating. Units: 10^7 m^3 s^{-2}

lar, enforcing axisymmetry eliminates all QG modes and reveals the SH element of the moist model; while introducing solstitial heating reverses the baroclinicity and produces a new (QGH) element with an easterly jet in the summer hemisphere; whereas adding diurnal heating at low Ω^* boosts the planetary waves and their impact on the natural-Hadley element and, in the limit, produces a Halley circulation. These specialized GCM states complement those of the basic parameter range discussed in Part I and, like them, have a variability that is limited to a few elementary forms.

The circulations in the moist AXISYMMETRIC set vary from a single, broad midlatitude jet in the Ω^* midrange to double jets — one in midlatitudes and one in low latitudes — in the high range. The meridional flows contain a primary pair of Hadley and Ferrel cells in the barotropic low latitudes and a secondary pair of cells in the baroclinic midlatitudes. The AXISYMMETRIC states can be partly understood in terms of the geometric argument of the first-order symmetric-Hadley (SH_1) theory, but only towards the pole and equator, not in midlatitudes. Differences occur because the AXISYMMETRIC flows are more inviscid, more nonlinear, and contain higher-order modes than their SH_1 counterparts. Latent heating increases the nonlinearity by intensifying the cells and by strengthening their coupling with the temperature field. As in the MOIST(8) case, the AXISYMMETRIC circulations fail to equilibrate simply when the Hadley cell becomes really narrow, as at $\Omega^* = 4$.

The AXISYMMETRIC and MOIST flows do not appear to be closely related to each other in general. In midlatitudes, the AXISYMMETRIC zonal flows greatly exceed the natural flows because a larger baroclinicity and thermal wind develop when the surface temperature is not fixed. Such AXISYMMETRIC jets are reduced toward the natural jets mainly by a barotropic instability, and so cannot provide the basic state for the MOIST baroclinic instability. In the high range, the AXISYMMETRIC system never has more than one midlatitudinal jet, so the MOIST $QG_{//}$ jets are obviously eddy driven. In low latitudes, however, the AXISYMMETRIC flow has some

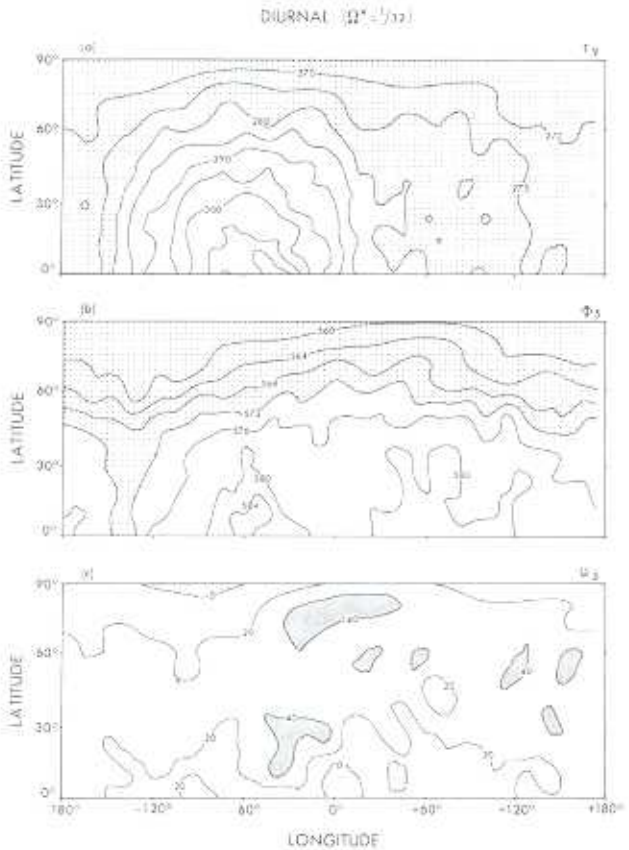

Fig. 30. Latitude-longitude distribution of the instantaneous (day 830) 990-mb temperature, and the 515-mb geopotential height and zonal velocity, in the diurnally heated DIURNAL model with $\Omega^* = 1/32$. Units: K, 10 m, ms^{-1}

connection with the QH element of the MOIST flows. But, paradoxically, the theoretical SH_1 modes relate more to the MOIST states than to the AXISYMMETRIC states — because the horizontal mixing limits the meridional nonlinearity in the natural system. Clearly, there is no unique symmetric-Hadley circulation, only a hierarchy of symmetric states of varying complexity determined by the rotation rate and by the various thermal, surface and subgrid factors.

The solstitial circulations in the OBLIQUE set contain the unstable easterly jet and vertically bimodal eddy momentum fluxes of the QGH element in the summer tropics, as well as the unstable westerly jet and poleward-traversing eddy momentum flux of the QG_γ element in the winter midlatitudes. These components are linked by an equator-straddling Hadley cell, a winter Ferrel cell, and wave propagation in the winter tropics. The scales of the jets and cells increase with θ_P and decrease with Ω^*, through the thermal Rossby number. An exceptional state at low Ω^* and high θ_P has a pole-to-pole Hadley cell, a warm winter pole and global easterlies — with thermal and momentum winds in the summer and winter hemispheres, respectively. When the tilt is low ($\theta_P = 10°$), the circulations have a mix of solstitial and equinoctial features in the summer hemisphere, with multiple QG_β jets arising at high Ω^*. The solstitial Hadley cell splits into two equi-

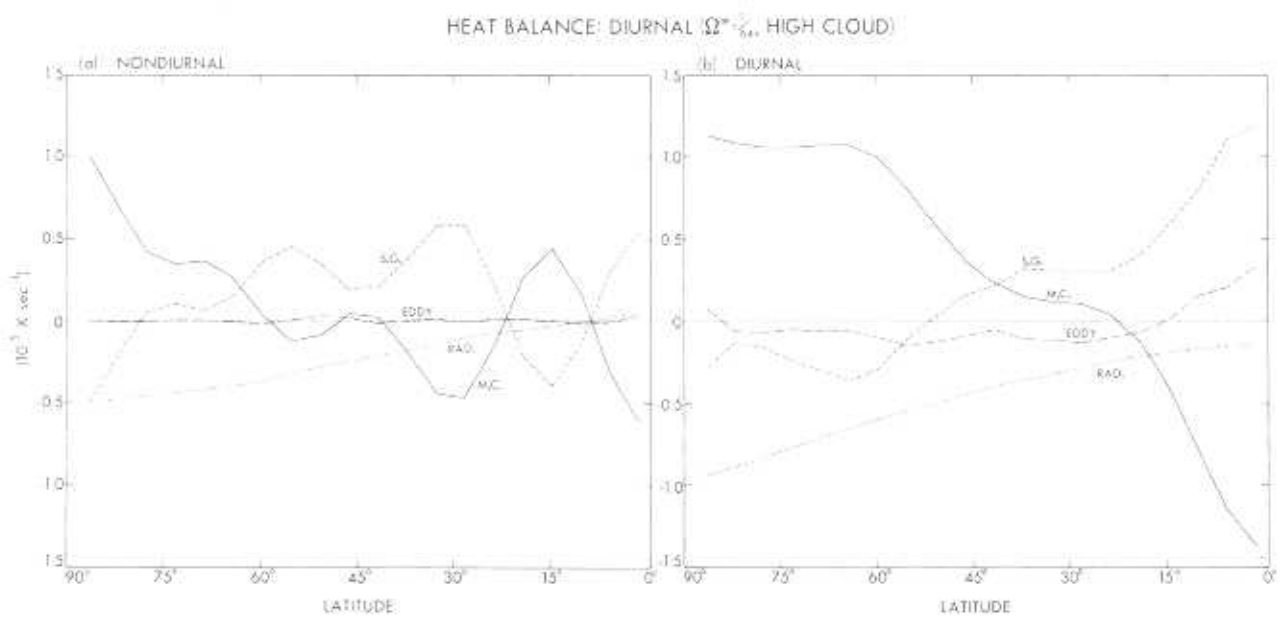

Fig. 31. Latitudinal distribution of the contributions to the mean rate of temperature change by the meridional circulation *(M.C.)*, the eddies *(EDDY)*, the radiation *(RAD)*, and the subgrid exchanges *(S.G.)* in the HIGH-CLOUD model with nondiurnal and diurnal heating for $\Omega^* = 1/64$. Units: 10^{-5} K s^{-1}

noctial Hadley cells when the obliquity drops below 5°.

The OBLIQUE circulations can be reasonably well explained theoretically: the mean flows closely resemble those predicted by the solstitial-symmetric-Hadley (SSH) theory — even though the theory involves a novel geometric argument and remains unproven — while the eddy fluxes of the winter QG_γ element can be understood in terms of an eddy cycle for the nonlinear baroclinic instability of a broad westerly jet (§ I-3.2). Furthermore, the bimodal momentum fluxes of the summer QGH element can be attributed (tentatively) to baroclinic instability aloft and to wave dispersion below. The QGH element is complex because the Hadley processes controlling the mean flow and the QG processes controlling the eddy fluxes both act in the same region. In the winter tropics, the fluxes arise from waves propagating out of the two instabilities, but the two contributions cannot be individually attributed, nor can the interaction between the two sets of waves be theoretically defined, as yet.

The diurnal heating influences the singular-range DIURNAL circulations mainly by boosting the planetary waves. The increased momentum flux then transforms the narrow polar jets of the NH elements into broad midlatitude westerlies. Following this diurnal transition at $\Omega^* = 1/16$, the circulations pass through two more transitions as $\Omega^* \to 0$: the asymptotic transition when the Hadley cell reaches the pole between $\Omega^* = 1/16$ and $1/32$; and the Halley transition when the eddies overwhelm the mean flow to give a subsolar-to-antisolar flow at $\Omega^* = 1/45$.

The DIURNAL singular-range eddies are not well understood. One theoretical approach to such Venus-like wave dynamics assumes that the Hadley $\bar{u}(\theta)$ field provides an equivalent Coriolis gradient β for a horizontal planetary wave propagation; another assumes that the Hadley $\bar{u}(z)$ field provides an equivalent Coriolis term f for a vertical inertial-gravity wave propagation. The planetary waves prevail in the DIURNAL circulations. The low-range and midrange circulations can be regarded, like the circulations of Venus and Earth, as combinations of SH modes and forced planetary waves, with the cause of the forcing (diurnality, baroclinicity) and the character of the waves differing with Ω^*. In the low range, the waves propagate away from the diurnally boosted tropical convection zones to create low-latitude westerlies; while in the midrange, they propagate away from the baroclinic zone to create midlatitude westerlies. Such theories, however, do not explain the steady-state circulations.

In fact, none of the circulations of Part II are as well explained as those of Part I — mainly because they occur at parameter extremes and deviate far from the terrestrial states for which the theory was primarily developed. They do, however, have implications for that theory: for example, the high-order AXISYMMETRIC modes imply that the QG and QH elements based on the SH_1 theory may only be first-order items; while the need for a different geometric argument for the SSH states throws doubt on the whole approach. The SH and SSH states are needed as non-arbitrary initial states for the equilibrated eddy cycles that define the elements. Eddy cycles cannot equilibrate or be considered self-consistent if the maintenance of the initial state is not considered. Thus the midrange QG_γ element is not fully defined by the calculations of Simmons and Hoskins (1978) because its jet is not self-sustaining, leading us to condition what we said in § I-1: the Lorenz problem is only partially solved. The high-range QG_β jet, however, has a self-sustaining momentum flux and is less dependent on the initial state, but it too lacks a full theory.

To make circulation theory more complete, the following problems need to be addressed (along with those listed in § I-7):

1) What are the symmetric-Hadley modes like for GCMs having a fixed surface temperature and no moisture? A hierarchy of SH solutions is needed to bridge the gap between the SH_1 theory and the higher-order AXISYMMETRIC states.

2) What forms do the equilibrated eddy cycles take for the hierarchy of SH basic states, at various Ω^*? This generalizes problem (1) of § I-7. At high Ω^*, such studies could show what happens when a barotropic instability pre-empts a baroclinic instability.

3) What are the solstitial-symmetric-Hadley modes like for the hierarchy of GCMs? These are needed to test the geometric argument of the SSH theory.

4) What forms do the equilibrated eddy cycles take for the SSH states, at various Ω^*? These are needed to relate the QGH fluxes to the baroclinic instabilities and the wave dispersion, and to define the interaction between the easterly and westerly jets.

5) What is the baroclinic instability of a tropical easterly jet like? The behavior of instabilities located in a Hadley cell is unknown but vital to the understanding of the QGH element.

6) What happens to wave propagation in the sin-

gular range? This could explain how modified NH elements evolve into Halley circulations.

7) How does the vertical structure influence the various QG and Hadley modes? To understand the planets, we need to know how deep or unbounded atmospheres differ from thin or bounded atmospheres in their dynamics.

8) And finally, we wonder if a unique invariant exists for global motion, and how the QG and Hadley modes can be disentangled to reveal it? The isomorphism between β-turbulence and SH circulations suggests that a more fundamental, more unified way may exist for describing global circulations. But this is, as yet, barely glimpsed.

The planets of the solar system can, in principle, provide unique tests of the various circulation theories in parameter regions untouched by Earth, over the full Ω^* range. Thus Mars can tell us about the easterly jet of the QGH element; Jupiter and Saturn, about the scale, interaction, and vertical structure of the QG and QH elements; Titan, about the seasonal variability of the symmetric-Hadley modes; Venus, about the diurnally modified NH element; while Uranus and Neptune have yet to divulge their significance.

We have now come to the end of our story and the patient reader may wonder what has been gained by touching upon so many subjects. Stated briefly, our concern has been with the synoptic and the specific, with defining the circulation range and isolating the circulation elements. In addressing this concern, we have gained perspective on Earth's atmosphere and extended dynamical theory into new parameter regions. When we began, we hoped — with much presumption — to encompass all of the planets in a single view, but this has proven premature given the limitations of observation and theory. Nevertheless, the basic thesis — that planetary variability is limited and defined by a few elementary forms, with species imposed by rotation and varieties allowed under structural and thermal diversity — is supported by the solutions. Although the demonstration is far from complete and the analysis is schematic and compressed, we have tried to seek out and define the remaining fundamental problems: for Earth, to explain the regional interactions; for the planets, to understand how the vertical structure and the depth influence the dynamical elements. Unified or not, the planets generalize and refine the meteorological paradigm.

Acknowledgements. I would like to repeat my thanks to those colleagues listed in Part I, especially to Leith Holloway for creating the GCM codes, and to Wendy Marshall for typing the final manuscripts.

References

Baines PG (1976) The stability of planetary waves on a sphere. J Fluid Mech 73:193–213
Eliassen A (1951) Slow thermally or frictionally controlled meridional circulation in a circular vortex. Astrophys Norv 5:19–60
Gill AE (1982) Atmosphere-ocean dynamics. Academic Press, New York
Hayashi Y (1974) Spectral analysis of tropical disturbances appearing in a GFDL general circulation model. J Atmos Sci 31:180–218
Held IM (1975) Momentum transport by quasi-geostrophic eddies. J Atmos Sci 32:1494–1497
Held IM, Hou AY (1980) Nonlinear axially symmetric circulations in a nearly inviscid atmosphere. J Atmos Sci 37:515–533
Hou AY (1984) Axisymmetric circulations forced by heat and momentum sources: a simple model applicable to the Venus atmosphere. J Atmos Sci 41:3437–3455
Hunt BG (1979a) The influence of the Earth's rotation rate on the general circulation of the atmosphere. J Atmos Sci 36:1392–1408
Hunt BG (1979b) The effects of past variations of the Earth's rotation rate on climate. Nature 281:188–191
Hunt BG (1982) The impact of large variations of the Earth's obliquity on the climate. J Met Soc Japan 60:309–318
Kutzbach JE (1985) Modeling of paleoclimates. Adv Geophys 28A:159–196
Leovy CB (1985) The general circulation of Mars: models and observations. Adv Geophys 28A:327–346
Lorenz EN (1969) The nature of the global circulation of the atmosphere: a present view. In: Corby GA (ed) The global circulation of the atmosphere. Roy Meteorol Soc:2–23
Manabe S, Mahlman JD (1976) Simulation of seasonal and interhemispheric variations in the stratospheric circulation. J Atmos Sci 33:2185–2217
Murray B, Malin MC, Greeley R (1981) Earthlike planets: surfaces of Mercury, Venus, Earth, Moon, Mars. Freeman, San Francisco
Pfister L (1985) Baroclinic instability of easterly jets with applications to the summer atmosphere. J Atmos Sci 42:313–330
Phillips NA (1954) Energy transformations and meridional circulations associated with simple baroclinic waves in a two-level, quasi-geostrophic model. Tellus 6:273–286
Rossow WB (1983) A general circulation model of a Venus-like atmosphere. J Atmos Sci 40:273–302
Rossow WB (1985) Atmospheric circulation of Venus. Adv Geophys 28A:347–379
Rossow WB, Williams GP (1979) Large-scale motion in the Venus stratosphere. J Atmos Sci 36:377–389
Schneider EK, Watterson IG (1984) Stationary Rossby wave propagation through easterly layers. J Atmos Sci 41:2069–2083
Simmons AJ, Hoskins BJ (1978) The life cycles of some nonlinear baroclinic waves. J Atmos Sci 35:414–432
Smith BA, Soderblom LA, Beebe R, 37 coauthors (1986) Voyager 2 in the Uranian system: imaging science results. Science 233:43–64
Webster PJ (1983) Large-scale structure of the tropical atmosphere. In: Hoskins BJ, Pearce R (eds) Large-scale dynamical processes in the atmosphere. Academic Press, New York, pp 235–275

Williams GP (1978) Planetary circulations: 1. Barotropic representation of Jovian and terrestrial turbulence. J Atmos Sci 35:1399–1426
Williams GP (1979a) Planetary circulations: 2. The Jovian quasi-geostrophic regime. J Atmos Sci 36:932–968
Williams GP (1979b) Planetary circulations: 3. The terrestrial quasi-geostrophic regime. J Atmos Sci 36:1409–1435
Williams GP (1985) Jovian and comparative atmospheric modeling. Adv Geophys 28A:381–429
Williams GP (1988) The dynamical range of global circulations-I. Climate Dyn 2:205–260
Williams GP, Holloway JL (1982) The range and unity of planetary circulations. Nature 297:295–299

Received August 28, 1986/Accepted April 27, 1988